Rapport

Development and verification of NDT for detecting voids in tendon ducts

Validation through mock-up specimens for post-tensioned concrete structures

Author(s):

Cosmin Popescu, Björn Täljsten, Kamal Raj Chapagain, Werner Bjerke, Jelena Zivkovic Tobias Danner, Rune Nilsen

Report no.: 2025:01222

Partner(s):

SINTEF

Rapport EXCON

Development and verification of NDT for detecting voids in tendon ducts

Validation through mock-up specimens for post-tensioned concrete structures

EMNEORD
Non-destructive testing, Post-tensioned concrete, Voids, Grouting

VERSJON
1

DATO
2025-12-30

FORFATTER(E)
Cosmin Popescu, Björn Täljsten, Kamal Raj Chapagain, Werner Bjerke, Jelena Zivkovic
Tobias Danner, Rune Nilsen

OPPDRAGSGIVER(E)
SINTEF

OPPDRAGSGIVERS REFERANSE
Tor Arne Hammer

PROSJEKTNUMMER
102028198/340843

ANTALL SIDER OG VEDLEGG
50

SAMMENDRAG
This report presents the development and verification of non-destructive testing (NDT) methods for detecting voids in tendon ducts of post-tensioned concrete structures. The work is based on laboratory testing using purpose-built mock-up specimens with documented internal conditions, allowing objective evaluation of NDT performance under controlled conditions. Ground-penetrating radar was verified as a reliable method for locating tendon ducts and defining geometry, forming the basis for targeted ultrasonic inspection. Ultrasonic methods showed clear sensitivity to entirely ungrouted duct sections, with detectability decreasing for greater duct depth, dense reinforcement, and multi-layer configurations. The results confirm that NDT is effective for identifying empty ducts, while interpretation uncertainty remains and is influenced by inspection strategy and operator competence. The mock-up program establishes a repeatable verification framework that supports method comparison and training, and provides a foundation for structured inspection workflows.

UTARBEIDET AV
Cosmin Popescu

SIGNATUR
Cosmin Popescu (21. jan.. 2026 11:23:22 GMT+1)

KONTROLLERT AV
Rune Nilsen

SIGNATUR
Rune Nilsen (22. jan.. 2026 10:48:43 GMT+1)

GODKJENT AV
Tor Arne Martius-Hammer

SIGNATUR

RAPPORT NR. 2025:01222
ISBN 978-82-14-07344-7
GRADERING Åpen
GRADERING DENNE SIDE Åpen

Historikk

VERSJON	DATO	VERSJONSBESKRIVELSE
1	2025-12-30	

Innholdsfortegnelse

BILAG/VEDLEGG

1 Introduction

1.1 Background

Post-tensioned (PT) concrete systems have been widely used in bridge construction since the late 1950s (Tinkey & Olson, 2007). These systems are favored for their economic efficiency, ability to span long distances, increased structural capacity, and relatively straightforward construction processes (Im & Hurlebaus, 2012). The technique involves installing steel tendons inside ducts—either internal or external to the concrete section—which are tensioned after the concrete has hardened, introducing a compressive force that counteracts tensile stresses.

The underlying concept of prestressing concrete is to overcome its inherent weakness in tension. Conventional reinforced concrete structures are prone to cracking under service loads, particularly due to bending moments caused by dead and live loads. These cracks reduce stiffness, increase long-term deformations, and expose reinforcement to corrosive environments. To mitigate these effects, compressive stresses are intentionally introduced into the concrete through prestressing techniques.

Prestressing can be implemented in two main ways:

1. **Pre-tensioning**, where the tendons are tensioned before casting the concrete.
2. **Post-tensioning**, where the tendons are tensioned after the concrete has cured.

This report focuses on the latter—post-tensioning—where tendons are threaded through ducts (typically made of metal or plastic), and stressed only after the concrete has gained sufficient strength. A key advantage of this method is the flexibility it offers during on-site construction, particularly the ability to implement curved tendon profiles. Curved tendons are essential in multi-span continuous bridges, where the cable path is typically elevated over supports (to resist negative moments) and lowered mid-span (to counteract positive moments), thereby optimizing internal force distribution.

However, a major vulnerability of post-tensioned systems arises after stressing: the exposed tendons must be protected against corrosion by injecting grout – typically a cement-based slurry – into the ducts. The purpose of the grouting is to bond the tendons to the concrete, prevent corrosion, and ensure long-term durability. If grouting is incomplete or poorly executed, it compromises the corrosion protection of the tendons and creates a potential safety risk.

This issue is at the heart of the current research effort. Incomplete grouting often leads to voids inside the tendon ducts, which in turn become potential initiation sites for corrosion. Detecting such internal voids non-destructively is a significant technical challenge. Direct visual inspection is typically impossible without invasive measures. However, recent advances in non-destructive testing (NDT) offer potential for detecting and mapping these voids indirectly, providing valuable input for structural condition assessment.

There is also a concern that extended lengths of ducts may be left ungrouted, which not only increases the risk of corrosion but may negatively affect load transfer mechanisms. The detailed structural implications of such unfilled ducts – especially on stress development, tendon anchorage, and duct-concrete interaction – will be explored in a subsequent chapter of this report.

The primary objective of the current work is to develop and verify NDT procedures for detecting voids in post-tensioned tendon ducts, with the goal of supporting practical and reliable condition assessments. To this end, the project employs specially designed mock-up specimens with known void configurations, enabling repeatable testing and robust verification of NDT methods under controlled conditions.

1.2 Objectives

The main objective of this work is to develop and verify systematic procedures for the application of non-destructive testing (NDT) methods in the detection of voids within tendon ducts of post-tensioned structures. This is achieved through the use of mock-up specimens specifically designed to simulate common defects observed in real structures.

To support this goal, the following sub-objectives have been established:

- **Develop systematic, verifiable procedures**
  The project aims to establish workflows for applying NDT methods, based on repeatable laboratory testing. Artificial voids are intentionally introduced in predetermined locations within mock-up specimens to create well-defined defect scenarios. This controlled setup enables objective evaluation of NDT equipment performance and method reliability.
- **Establish step-by-step guidelines for defect detection**
  Through repeated testing and iteration, the project seeks to define practical, step-by-step guidelines that practitioners can follow to identify and interpret signals associated with typical tendon duct defects. These procedures will serve as a foundation for future field application and standardization.
- **Enable hands-on training and knowledge transfer**
  The mock-up specimens provide an opportunity for training NDT operators in a controlled environment. Practitioners can test and refine their skills by comparing NDT results with known defect locations, which is rarely possible in field conditions. This not only improves operator competence but also promotes consistent interpretation across teams and organizations.
- **Bridge the gap between lab validation and field implementation**
  While this report focuses on laboratory-based validation using mock-ups, the methods developed will later be applied in real bridge inspections. Field test results will be presented in a separate report, allowing for a clear distinction between controlled verification and field adaptation.
- **Address multiple infrastructure types**
  The mock-up specimens used in this project are representative not only of bridge structures but also of offshore concrete elements, broadening the relevance and applicability of the developed methods.

2 Literature review and existing practices

2.1 Importance of grouting and risks of voids

In post-tensioned concrete structures, grout serves three critical functions: it protects prestressing tendons from corrosion, provides bond between the tendon and surrounding concrete, and contributes to the system's stiffness and effective force transfer. However, construction records and field inspections from various bridge inventories have consistently revealed instances of poor or incomplete grouting, resulting in voids within the tendon ducts. These voids – filled with air, bleed water, or moisture – undermine all three functions and significantly compromise structural integrity. Incomplete grouting and voids in tendon ducts have been identified as a major durability risk in post-tensioned structures (Sharma et al., 2024).

Voids expose prestressing strands to oxygen and chlorides, creating an environment conducive to corrosion. This is particularly hazardous in aggressive environments such as coastal regions or areas with frequent use of de-icing salts. Studies and documented failures in both Europe and the U.S. have linked voids directly to cases of tendon rupture and sudden structural degradation. According to (Menga et al., 2023), incomplete grouting is the predominant root cause of corrosion in post-tensioned systems. The problem is most acute at typical weak points in the tendon layout – such as high points, curved ducts, and anchorage zones – where air naturally collects and grout flow is more difficult to control.

The corrosion that initiates in these regions often leads to severe pitting and localized section loss in the steel strands. Because this type of degradation progresses internally and without surface indicators, it often goes undetected until a sudden and brittle rupture occurs. When a single strand fails in an ungrouted region, force redistribution becomes highly unreliable, potentially triggering progressive failure of neighboring tendons. This mode of failure has been observed in structures as early as 10–20 years into service – far earlier than the intended design life – demonstrating the severe durability risks posed by ungrouted voids. Characteristics of strand corrosion are provided in Figure 1.

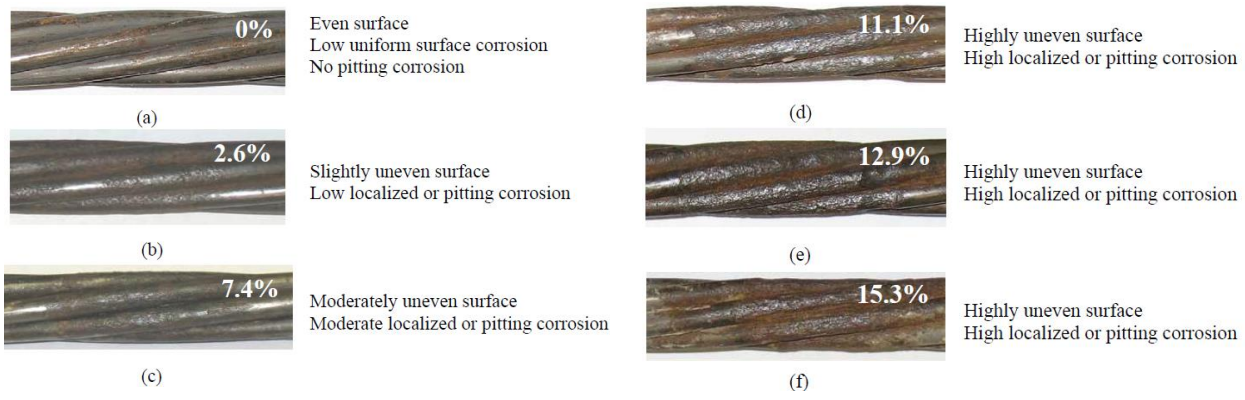

Figure 1. Photographs showing corrosion level and surface characteristics of strands. (Trejo et al., 2009)

Two primary causes of corrosion are identified in the literature:

2.1.1 Segregated or defective grout

This phenomenon is characterized by the appearance of a white, soft, unhardened paste – an exudation product that separates from the intended grout mix. Such exudate is highly enriched in water and sulfates and exhibits an extremely high pH, often between 13 and 14 (Carsana & and Bertolini, 2015). Though cementitious, this segregated material fails to protect the strands and instead becomes an aggressive corrosive medium. Laboratory and field investigations have shown that strands in direct contact with this material suffer from localized corrosion, particularly pitting (Bore et al., 2010; Carsana & and Bertolini,

2015). The combination of high alkalinity and ionic content fosters deep corrosion pits, acting as notches that concentrate stress.

Wet segregated plastic grout (Lau et al., 2013)

Soft and wet grout (Popescu et al., 2024)

Figure 2. Examples of segregated and defective grout observed in post-tensioned tendon ducts

This localized degradation significantly weakens the steel, increasing the likelihood of brittle fracture without prior visible damage. In one documented case, a tendon failed in under two years due to such conditions (Bore et al., 2010; Carsana & and Bertolini, 2015). The corrosive action is exacerbated in high-strength prestressing steels, which are notably more sensitive to pitting and hydrogen-related cracking than conventional reinforcement. As explained by (Nürnberger, 2002), such strands under tension are vulnerable to stress-corrosion cracking, hydrogen embrittlement, and corrosion fatigue, especially when exposed to aggressive bleed water environments. This bleed water, often trapped during construction, may contain high concentrations of sulfates, chlorides, and potassium ions, all of which contribute to the corrosive potential. Once corrosion initiates in these strands, even small pit depths (e.g., 0.2–0.6 mm) can dramatically reduce their mechanical performance, making rupture under service loads much more likely (Nürnberger, 2002).

2.1.2 Voids due to grouting errors

The second, and more prominent, cause of corrosion in post-tensioned tendons is the presence of voids in the grout. These voids can form due to several issues such as entrapped air pockets, grout bleeding, or improper grouting procedures (Im & Hurlebaus, 2012). Air voids may be trapped if the grouting vents are closed too early – before the ducts are completely filled – or as a result of air naturally migrating toward the high points in the tendon duct system, often located near anchorages (Cavell & Waldron, 2001). Additionally, grout bleeding allows water to separate from the grout mixture. This water can move along the interface between wire strands and eventually accumulate near anchorages where it may evaporate, leading to increased risk of corrosion (Hansen, 2007).

Void inside tendon duct and corrosion on the strands (Popescu et al., 2024)

Void inside tendon duct and corrosion on the strands (Holmqvist et al., 2024)

Partially filled duct (Holmqvist et al., 2024)

Empty duct (Holmqvist et al., 2024)

Figure 3. Examples of voids and missing grout in post-tensioned tendon ducts

Regardless of the specific cause, the presence of these voids leads to two primary concerns. First, the prestressing strands within these voids remain ungrouted and are thereby exposed to environmental aggressors, particularly chlorides. These chlorides can penetrate from external sources such as de-icing salts or seawater spray and also from airborne marine aerosols or chloride-rich construction materials like sand used in concrete production (Cavell & Waldron, 2001; Minh et al., 2007; Nürnberger, 2002). Once these aggressive agents reach the exposed steel surface, localized corrosion (especially pitting) may occur, which drastically reduces the fatigue resistance and load-bearing capacity of prestressing steel—even at small corrosion pit depths of 0.2–0.6 mm (Nürnberger, 2002). Moreover, in crevice-like environments such as those formed by voids or poor grout contact, the risk of hydrogen-induced stress corrosion cracking (H-SCC) increases, especially under tensile stress conditions typical in post-tensioned systems (Nürnberger, 2002).

Second, the presence of voids prevents the intended mechanical interaction between the grout and the prestressing strands. If a strand breaks, proper stress redistribution to neighboring strands cannot occur unless the grout is continuous and in full contact with the steel. This lack of redundancy in the load path may lead to disproportionate failures, especially near anchorage zones where the stresses are highest (Martin et al., 2001).

Although limited research exists that directly quantifies the effect of grout voids alone on the ultimate load-carrying capacity of post-tensioned members, most studies suggest that voids primarily become critical when combined with corrosion. In such cases, the resulting loss of cross-sectional area and prestressing force in the tendons significantly compromises structural integrity. In otherwise intact,

grouted systems, even if a strand fails, the surrounding grout may enable a re-anchoring mechanism—an effect observed in controlled demolitions. This re-anchoring allows the fractured tendon to regain some anchorage in the grout and partially restore the prestressing force.

Experimental observations from controlled demolition of post-tensioned bridges (Buchner & Lindsell, 2004) and tests involving deliberate tendon cuts (Belhadj & Waldron, 1993; Dai et al., 2021; Felstead & LINDSELL, 1981) confirm that such re-anchoring behavior can occur in fully grouted ducts. However, the effectiveness of this mechanism strongly depends on the grouting condition: full grouting can facilitate re-anchoring, whereas completely ungrouted or partially grouted ducts inhibit it.

(Wang et al., 2014) also found that insufficient grouting has minimal influence on the initial, linear-elastic response before cracking. Once cracking initiates, however, grout deficiencies lead to reduced section stiffness, lower ductility, and a decrease in ultimate flexural strength. Therefore, while grout voids alone may not drastically affect the structure in the uncracked state, their presence in combination with tendon rupture represents a dangerous scenario. Such cases must be carefully considered when evaluating the residual capacity of post-tensioned members.

Given the role of grout in ensuring both the durability and mechanical performance of post-tensioned systems, the presence of voids within tendon ducts emerges as a critical vulnerability – effectively the root cause behind many long-term service issues. Voids not only negate corrosion protection but also disrupt force transfer mechanisms and compromise redundancy in the event of tendon rupture. These problems are particularly concerning because they develop invisibly, without external indications, and are often discovered only after substantial deterioration has occurred. Traditional inspection techniques fall short in addressing this hidden threat, leaving NDT as the only viable solution for timely identification and assessment of internal voids. However, the effectiveness of NDT depends not just on the hardware used, but equally on the post-processing methods and the interpretive skill of the human operator. Variability in detection accuracy can result from inconsistent application, lack of training, or insufficient calibration against known conditions. Therefore, the present study is both timely and necessary – it aims to validate NDT techniques under controlled conditions, develop repeatable testing procedures, and create step-by-step guidance for interpreting results. By doing so, this work addresses a major gap in current inspection practices and contributes toward safer, more reliable condition assessments of post-tensioned concrete infrastructure.

2.2 Detection of voids in tendon ducts: existing methods

Post-tensioned (PT) concrete systems present unique challenges for NDT, particularly in detecting voids within grouted ducts. The presence of tendons inside metallic ducts, often embedded in large cross-sections or covered with overlays, limits the effectiveness of surface-based techniques. Despite these difficulties, the literature has explored and applied a variety of NDT methods for internal void detection. Common approaches include Ground Penetrating Radar (GPR), Ultrasonic Pulse Echo (UPE), Impact Echo (IE), Radiography, and newer hybrid or tomographic methods. Each method offers certain advantages and limitations depending on duct accessibility, materials, geometry, and signal clarity.

Challenges of detecting internal defects

1. Duct material and geometry

Metallic ducts attenuate or reflect signals, reducing effectiveness of some techniques (e.g., GPR). GPR relies on the propagation of high-frequency electromagnetic waves, which reflect at boundaries where there is a significant change in dielectric properties. When these signals encounter a metallic duct, the contrast in electrical conductivity between concrete and steel is so high that nearly 100% of the electromagnetic energy is reflected at the duct's outer surface. This reflective behavior causes the duct to act like a mirror, preventing the waves from penetrating into its interior. Consequently, while GPR can

accurately detect the location and alignment of metallic ducts, it cannot reveal the internal condition—whether the duct is fully grouted, partially voided, water-filled, or affected by internal corrosion.

Regarding duct geometry, while it does not inherently prevent detection, it introduces practical complexities. Curved tendon profiles, which are common in multi-span post-tensioned structures, require multiple scans to accurately trace the tendon path. As shown in Figure 4, each scan provides only a sectional view of the duct layout. Without sufficient spatial coverage, it becomes difficult to reconstruct the full tendon profile, especially when they deviate from straight lines or interact with surface reinforcement.

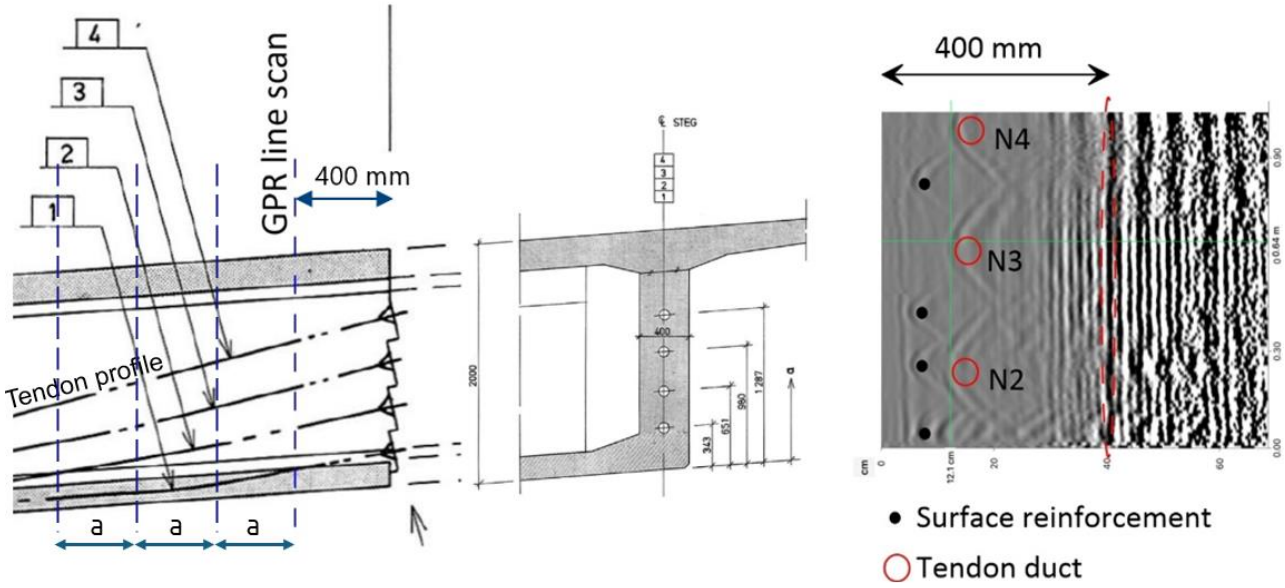

Figure 4. Example of GPR scan slices spaced (a) used to reconstruct curved tendon profiles

Interpreting these results demands experience and careful alignment of signal reflections across several scan slices or views**.** However, accurate reconstruction of the tendon profile requires more than just correlating signal patterns across multiple scans. Reflections detected by GPR may correspond to either tendon ducts or conventional reinforcement (see Figure 4), and distinguishing between the two can be complicated.

To resolve these ambiguities, a third critical input is often necessary: reference to original or idealized as-built drawings. These drawings help validate the expected tendon layout and improve the accuracy of interpretation. This introduces added complexity, as correct analysis requires not only NDT expertise but also a solid understanding of post-tensioning design and the ability to interpret structural drawings accurately. Failure to correctly identify tendon locations may result in an incorrect tendon profile, which can have implications in subsequent steps. For instance, if ultrasonic or other focused testing is applied based on a misidentified duct location, it may yield irrelevant results. Worse, if invasive verification such as coring is attempted in the wrong location, there is a real risk of unintentionally intersecting an active tendon. Thus, while not a fundamental barrier, it does demand a more rigorous and structured scanning strategy to ensure reliable results.

2. Access limitations

Post-tensioned ducts are frequently embedded deep within massive concrete elements or situated in locations that are physically difficult to access – such as the corners of box girders or zones where ducts pass over supports. These areas are often further obstructed by concrete overlays, asphalt surfacing, or other structural components. Additionally, a shadowing effect can occur when multiple ducts are installed

in parallel: signals may be partially or fully blocked by the first duct, rendering it difficult or impossible to assess ducts positioned directly behind.

As illustrated in Figure 5, the left side shows ducts embedded in the upper deck slab – the traffic-bearing surface – while the right side shows ducts in the bottom slab, which is accessible from inside the box girder. Typically, inspectors have physical access only from the inside of the box-girder, unless external scaffolding or lifting platforms are used.

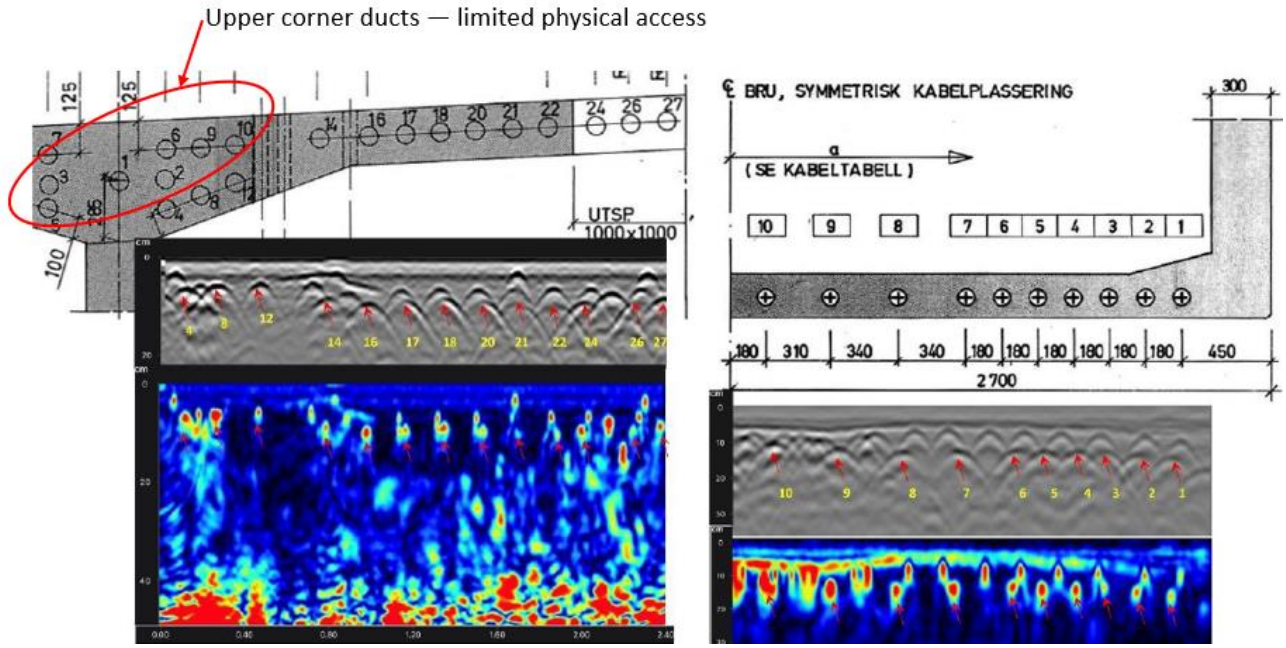

Figure 5. Cross-section of a post-tensioned box girder segment (top) with corresponding GPR scan results (bottom)

Access to the upper tendon zones, especially those placed near the deck-web intersection (corners of the box girder), is severely constrained. These areas are covered by asphalt surfacing, which limit physical access. Ducts positioned near the deck–web intersection are inaccessible from within the box girder and typically cannot be inspected from above without traffic disruption, making them effectively uninspectable without major intervention.

Moreover, as seen in the GPR scans in Figure X, even when scanning is possible, signal strength is highest from ducts closest to the surface. Ducts positioned deeper, especially those obscured by other layers or reinforcement or ducts, suffer from attenuation or signal shadowing. This limits the ability to assess all tendon paths reliably.

3. Signal interference

In regions where tendon ducts are closely spaced – particularly around corners or congested zones – the ability to distinguish individual ducts using NDT methods becomes significantly reduced. Reflections from adjacent tendons may overlap, producing signal clusters that are difficult to interpret with confidence (see Figure 5). Moreover, not all anomalies detected in the scan are directly related to tendon defects. Signal patterns can also be influenced by previous repair zones**,** delaminations, or defects in the parent concrete, such as honeycombing or segregation pockets near the duct. These features can mimic the signal response of voids or grouting deficiencies, leading to false-positive indications**.**

4. Resolution and sensitivity

Given the current state of practice, it remains difficult to reliably distinguish between poor-quality grout**,** partially filled ducts, and completely voided sections using available NDT methods. While both ultrasonic and electromagnetic techniques are generally effective in detecting the presence of anomalies, they often lack the resolution or interpretive confidence needed to assess the size, type, or severity of the defect. As a result, a signal anomaly may indicate anything from minor grout segregation to a fully empty duct, but this cannot be determined with certainty. This limitation increases the need for exploratory verification, making it almost mandatory to confirm NDT findings through targeted coring and endoscopic inspection. Without such follow-up, it remains difficult to confidently assess the true condition of the tendon duct.

In addition to the general limits of spatial resolution, there is also uncertainty in the precise location of detected anomalies within the duct cross-section. Tendons are not always centered within their ducts; they may rest eccentrically, pressed to one side. In such cases, if a void is located behind the tendon (relative to the accessible face), it may still be detected by ultrasonic methods. However, confirmation using endoscopy becomes extremely difficult. Coring from the same side will typically strike the tendon bundle before reaching the void, making it nearly impossible to visually validate the anomaly. This limitation is not a failure of detection per se, but a limitation in verification due to restricted access and spatial interpretation. It underscores the challenge of relying on one-sided access in box girders and highlights the need for caution when dismissing NDT findings that cannot be intrusively confirmed.

5. Human Factors and Operator Dependence

Inspections of post-tensioned structures are often carried out in difficult environments—at height, sometimes over open water, and frequently under harsh weather conditions. These structures typically require scaffolding (Figure 6), which limits both working time and physical comfort for proper data collection and review. Inside box girders (Figure 6), inspectors may need to operate in cramped positions, kneeling or sitting for prolonged periods in order to scan all relevant areas. In larger sections, mobile scaffolding is frequently used to reach high-placed ducts. Inspectors often have to operate with equipment held overhead, arms fully extended above shoulder height, which introduces significant physical strain and limits both precision and endurance. This setup not only slows down the inspection process but also increases the risk of incomplete data collection due to operator fatigue or limited maneuverability.

Figure 6. Practical challenges during NDT inspections of post-tensioned bridges, including access via scaffolding above water, confined interior spaces, and overhead scanning in constrained positions

Under such constraints, inspectors may experience fatigue and time pressure, increasing the likelihood of rushed decisions and reduced accuracy, particularly when evaluating unclear or ambiguous signal patterns.

In addition, modern NDT equipment often depends on tablets or smart devices for data acquisition and visualization. While convenient, these devices are prone to rapid battery drain in cold conditions, which can interrupt inspections or result in loss of real-time feedback.

Given these factors, it is evident that NDT results are highly dependent on the operator's skill and experience. To improve consistency and reliability, there is a growing need for structured inspection protocols, hands-on training with realistic mock-ups, and robust post-processing tools that can assist or validate field interpretations.

2.3 Basis for current study: Findings from H3.1

A detailed review of NDT methods was conducted within work package H3.1. The evaluation included a wide range of techniques with respect to parameters such as field readiness, sensitivity to voids, portability, safety, and ease of interpretation.

Based on that review, a shortlist of practical and technically suitable methods was identified for further testing and verification within H3.3. The selection of NDT methods prioritized for further development in this project was guided by several practical and technical criteria. First, field applicability was considered essential; all selected techniques needed to function effectively under typical site constraints, such as limited access inside box girders, work at height, or time-restricted inspections performed from scaffolding. Portability and ease of setup were thus important factors. Equally important was the sensitivity of the method to internal duct anomalies. The ability to detect voids – whether air-filled, water-filled, or associated with poor grout quality – was prioritized. Since no single method is flawless, the value of combining complementary techniques was also emphasized. For example, GPR may be used for duct location and profiling, while ultrasonic or impact echo methods provide a more direct indication of void presence. This multi-method approach allows cross-validation of findings, improving reliability and reducing the risk of false positives or negatives. Another critical criterion was the interpretability of the collected data. Methods that provide clear signal outputs, imaging, or patterns that can be consistently interpreted were favored over those requiring overly subjective analysis. However, the role of human operators remains vital. Therefore, techniques were preferred that support structured training and repeatable workflows, minimizing dependency on individual intuition or highly specialized expertise.

Safety and intrusiveness were also factored into the selection process. Preference was given to techniques that are non-invasive, pose minimal health risks, and ideally require access from only one side of the structure – a common limitation in bridge inspections. Finally, the level of technological maturity and commercial availability was considered. The selected methods had to be sufficiently developed and available for practical deployment, even if further procedural refinement is needed for specific applications.

Collectively, these criteria ensured that the methods chosen for testing and verification under H3.3 offer not only technical capability but also practical applicability in real-world settings – supporting the long-term goal of standardized, field-ready procedures for void detection in post-tensioned structures. The intention is that these techniques can be directly applied in the case studies presented in a separate project deliverable.

These include:

- **Ground Penetrating Radar (GPR):** Used to locate the tendon ducts and reconstruct their profile prior to further testing. Although limited in its ability to detect internal duct conditions in metallic sheaths, it provides critical spatial orientation and mapping, especially in curved or congested zones.
- **Ultrasonic Pulse Echo (UPE) and Ultrasonic Tomography (both transverse and longitudinal waves):** These were identified as the primary candidates for detecting voids and irregularities

inside ducts. Their ability to detect changes in material stiffness and discontinuities made them promising for initial screening.

- **Impact Echo (IE):** Considered a complementary method to help narrow down the areas of interest identified by ultrasonic methods.

While other methods such as radiography, muon tomography, and acoustic emission, were reviewed, they were deemed less feasible due to safety concerns or complex interpretation requirements. These techniques remain of academic interest but are not prioritized for field deployment in this phase of the project.

2.4 Mock-Up specimens in NDT verification: Insights from past studies and basis for the present work

Mock-up specimens are widely recognized as essential tools for verifying and evaluating NDT methods, particularly in the context of complex structures such as post-tensioned concrete elements. Several research groups and infrastructure agencies have over the years developed and tested such specimens to better understand the reliability, limitations, and practical challenges of applying NDT in real-world scenarios. By reviewing these previous initiatives, it becomes evident that while mock-ups can greatly enhance our ability to benchmark NDT techniques, their design and implementation must be handled with care to ensure meaningful results.

This chapter provides an overview of these reference projects and discusses how their outcomes informed the design choices for the current mock-up. By learning from the limitations observed in other studies, this work aims to contribute more robustly to the development of reliable NDT procedures for the inspection of prestressed concrete structures.

2.4.1 Test 1: (Wiggenhauser et al., 2015)

One example is the mock-up campaign carried out by (Wiggenhauser et al., 2015) on steel-concrete modules intended for nuclear power plant applications (Figure 7). The aim was to evaluate acoustic-based NDT methods for detecting embedded voids and assessing the feasibility of inspecting such composite elements, where concrete is enclosed between steel liners.

Without going into detail about the specific test results, which fall outside the scope of the current campaign, it is important to highlight the key lesson: while the small mock-up fulfilled its role as a testing ground for defect detection in bare concrete, it did not fully deliver on its purpose of simulating the more challenging steel-concrete interface conditions encountered in real structures; the limitations of wave propagation through steel and the dominance of reflections from welds and edges significantly reduced measurement reliability.

From a broader perspective, the campaign demonstrated that mock-up design needs to be not only *realistic* but also *constructively honest* about the conditions it aims to simulate. Several recommendations were made: larger mock-ups to reduce surface interference; better control of defect types, sizes, and positions; inclusion of complex interfaces such as delaminated zones; and new ultrasonic systems specifically developed for testing through steel.

Figure 7 Fabrication of mock up specimens (from (Wiggenhauser et al., 2015))

2.4.2 Test 2: (Giannini et al., 2020)

Another mock-up campaign was led by (Giannini et al., 2020) focusing on alkali-silica reaction (ASR) damage in plain concrete. Unlike earlier studies limited to small-scale mortar bars, this effort aimed to create larger, standardized concrete slabs with known levels of ASR-induced deterioration. The purpose was not to validate a specific method, but to provide a shared platform for assessing the viability of different NDT techniques under conditions more representative of field structures.

Without going into test results, which are beyond the scope of this work, the main takeaway is that the mock-ups largely achieved their goal. Each slab was conditioned to a target expansion (0.05%, 0.10%, 0.20%) and stored in controlled environments, providing a solid basis for inter-laboratory comparison.

Nonetheless, the campaign exposed key challenges. The larger slabs continued expanding after shipment, while smaller prisms shrank due to different storage conditions, complicating efforts to maintain distinct damage states. Delays in testing access also meant some measurements were taken well after the intended conditioning phase.

The broader lesson is the difficulty of balancing realism and control in mock-up design. While the specimens successfully simulated various ASR stages, sustaining stable damage levels over time proved difficult. Future efforts should account for how deterioration may evolve both during and after conditioning, especially when aiming to simulate progressive degradation.

2.4.3 Test 3: (Dethof & Keßler, 2024)

A third example comes from a study authored by (Dethof & Keßler, 2024) which focused on the simulation-based design and ultrasonic testing of concrete mock-ups with embedded defects. The aim was to explore how numerical modelling can guide the design of diagnostically useful specimens, particularly for evaluating the detectability of honeycombs.

The mock-up included embedded reinforcement, steel pipes, and cast-in honeycombs. Finite element simulations were used beforehand to predict how ultrasonic waves would interact with these features, helping to optimize their placement and spacing. This approach minimized signal interference and enhanced interpretability during testing.

Importantly, the study also included ultrasonic inspections, with results presented and evaluated. A key finding was that even well-designed honeycombs could be difficult to detect in practice, depending on their geometry and surrounding material. This highlighted the need for mock-ups that not only simulate realistic flaws but also provide meaningful diagnostic challenges.

The main lesson is that combining simulation-driven design with physical testing improves both the quality and relevance of mock-ups. These insights were used in designing the present mock-up to ensure that the embedded features are both representative and easy to interpret during testing.

2.4.4 Test 4: (Oh et al., 2024)

In another campaign by Mihashi et al. focused on evaluating the performance of different NDT methods in detecting internal delamination in reinforced concrete. The specimen, representing a typical concrete bridge deck with an asphalt overlay. Delaminations were simulated by embedding inserts made of plastic film and mesh at varying depths – between the overlay and deck, above the top reinforcement, and below the bottom reinforcement – reflecting locations where such defects commonly occur in practice. The mock-up was designed with long-term use in mind, stored outdoors to allow natural exposure to freeze–thaw cycles. This added a layer of surface deterioration, providing a semi-realistic context for testing. Importantly, the design allowed for controlled and repeatable delamination simulation, offering a platform for method comparison.

However, the approach also highlighted some inherent trade-offs. While the artificial inserts allowed for precise control over location and geometry, they remained idealized and may not fully capture the material complexity or irregularity of naturally developed delamination. Additionally, the use of plastic materials to simulate air gaps simplifies the condition but does not replicate mechanical debonding or moisture influence present in actual field cases. The key takeaway from this study is the value of deliberately simplified yet well-documented specimens for benchmarking.

2.4.5 Test 5: (Krause et al., 2008)

Another significant mock-up campaign, reported by Washer et al., aimed to evaluate the ability of ultrasonic methods to detect voids in grouted post-tensioning ducts embedded in concrete. The specimen included metallic ducts with known internal conditions: fully grouted, partially grouted, and ungrouted segments (Figure 8). These ducts were embedded in a reinforced concrete block to realistically reflect the geometry and material constraints of in-situ bridge components.

Several practical and conceptual lessons emerged from the mock-up effort. First, the study demonstrated the critical importance of embedding ducts within concrete, rather than testing them in isolation. The steel-concrete interface had a clear influence on wave propagation and signal interpretation, and without this structural context, test results would have lacked field relevance.

Second, the campaign highlighted the benefit of having well-documented internal ground truth, allowing the researchers to evaluate method sensitivity and reliability under controlled conditions. However, it also showed that the simplified void geometries used in the mock-up — often clean and uniform air gaps — did not fully capture the irregular shapes, moisture presence, or partial bonding often observed in real voids. This limited the ability to generalize the detection thresholds to actual structures.

Figure 8 Left: Tendons being installed in the Large Concrete Slab (LCS) prior to grouting. Right: Close-up of a tendon duct containing prestressing strands with an intentionally created artificial void, prepared before placement in the slab.

2.4.6 Test 6: (Kessler & and Grosse, 2023)

This study, presented by (Kessler & and Grosse, 2023), focused on integrating a mock-up into civil engineering education to provide students with hands-on experience in NDT. Unlike mock-ups designed primarily for research or method benchmarking, this initiative prioritized training, accessibility, and realism in an academic setting. A reinforced concrete slab (Figure 9) was constructed with deliberately embedded features – including plastic and steel elements – to mimic internal heterogeneities and allow testing with methods such as ultrasonic pulse echo, radar, and impact-echo.

The mock-up served as a versatile educational tool. It was designed for repeated use across multiple training sessions, and its layout was well-documented to enable effective interpretation and comparison of results. One of the key outcomes was the recognition that physical mock-ups enhance conceptual understanding of wave propagation, reflection, and practical testing constraints far more effectively than simulations or theoretical exercises alone.

The study underscored that even relatively simple specimens can offer substantial educational value, especially when their geometry and embedded features are thoughtfully planned to challenge interpretation without overwhelming students. Although the specimen was not built to represent deterioration in field structures, it succeeded in meeting its goal of teaching inspection techniques and reinforcing key diagnostic concepts in a controlled, repeatable environment.

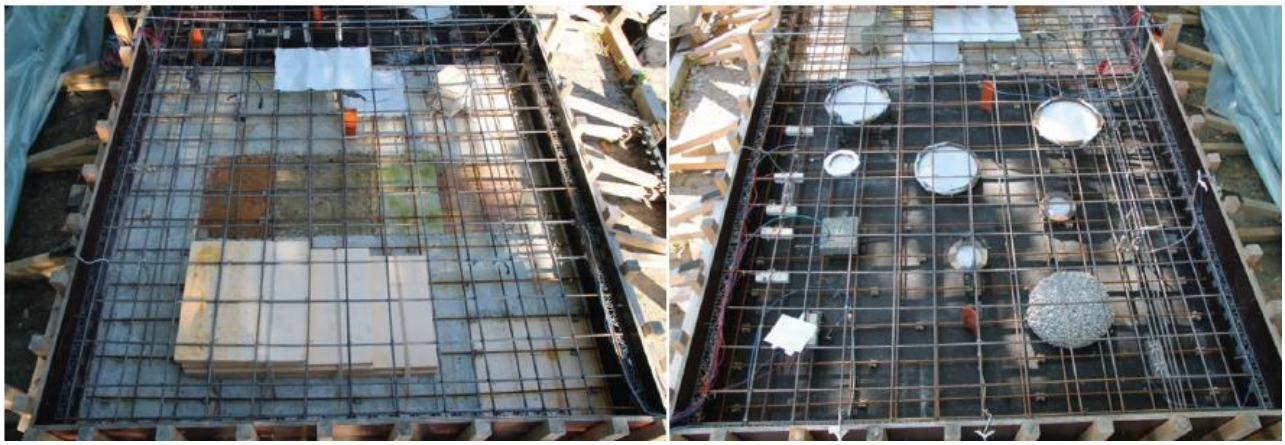

Figure 9 Photos of the mock-up before concreting

2.4.7 Test 7: (Popescu & Täljsten, 2020)

(Popescu & Täljsten, 2020) developed a mock-up specimen to evaluate NDT techniques for detecting internal defects in tendon ducts, including grouting voids, water ingress, and corrosion indicators. The reinforced concrete specimen included a combination of steel and plastic ducts**,** tendons, and a series of engineered defects, such as water-filled bags, rubber inserts, ungrouted sections, and corrosion zones. The aim was to reflect the wide range of conditions encountered in real post-tensioned structures, offering a high level of realism and material diversity.

While the mock-up succeeded in simulating realistic conditions, several important lessons emerged. One of the key takeaways was that increased complexity does not always lead to better outcomes – particularly when the mock-up is used for training personnel or evaluating specific NDT equipment. When too many defect types are combined in close proximity, interactions between defects can distort signals and make it difficult to isolate the performance of individual methods or interpret results clearly. In effect, the setup can become more complicated than what would typically be found in situ on a real bridge, undermining the clarity needed for controlled testing or instructional purposes.

This experience highlighted that while realistic features are essential for field-relevant validation, mock-up design should be guided by a clear purpose – whether it is to simulate field conditions, evaluate equipment sensitivity, or train operators. Each goal may demand a different balance between realism, simplicity, and control.

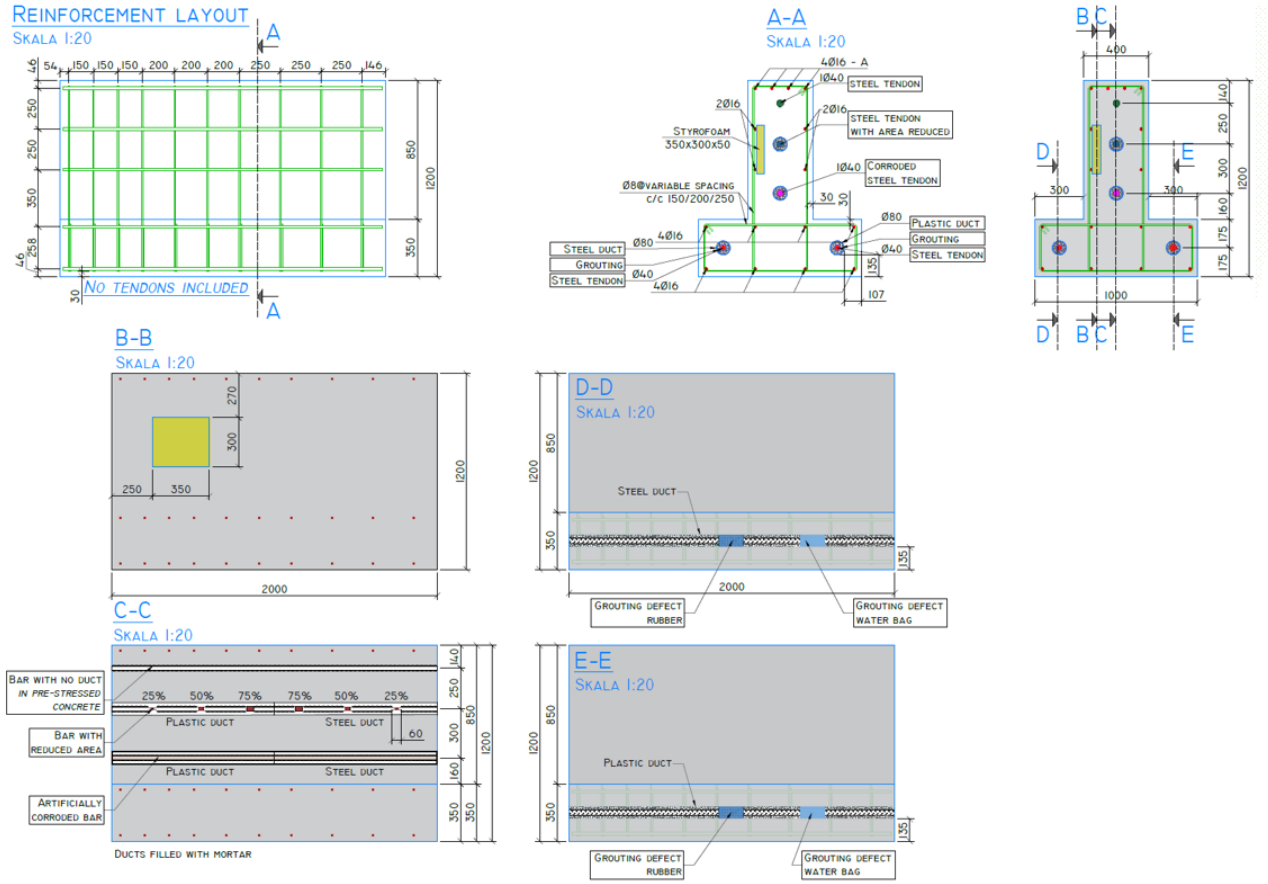

(a)

(b) (c) (d) (e) (f)

Figure 10 Design (a) and fabrication process: (b–c) Water bags and rubber inserts simulating water ingress and grouting defects inside tendon ducts; (d) grouting of the ducts; (e) placement of all ducts, reinforcement, and artificial defects before concreting; (f) completed mock-up specimen.

In planning the present mock-up specimen, these lessons were taken into careful consideration. The design phase emphasized clarity and traceability, with detailed documentation of the reinforcement layout, embedded duct configurations, and intended defects. Particular attention was given to ensure that known errors in earlier campaigns – such as overlapping reinforcement causing signal confusion or lack of ground truth – would be avoided. The goal was to create a specimen that is not only representative of field conditions but also reliable as a testbed for method verification and comparison.

3 Methodology

3.1 Mock-Up Specimen Design

To assess the applicability of non-destructive testing (NDT) methods in detecting voids and anomalies typically encountered in post-tensioned concrete structures, four custom-designed concrete mock-up specimens were fabricated. Each specimen was tailored to reflect specific defect types under controlled conditions, allowing for repeatable validation of inspection techniques.

3.1.1 Specimen 1

The first mock-up specimen was designed as a baseline concrete element to support the calibration and verification of NDT methods aimed at detecting internal reinforcement and evaluating material properties.

The specimen measures 1600 × 1200 × 300 mm and is reinforced with Ø16 mm bars placed in both the top and bottom layers. The reinforcement spacing is 100 mm and 200 mm center-to-center, arranged in orthogonal directions. The clear cover to the rebar is approximately 35 mm. No ducts or embedded defects were introduced in this specimen.

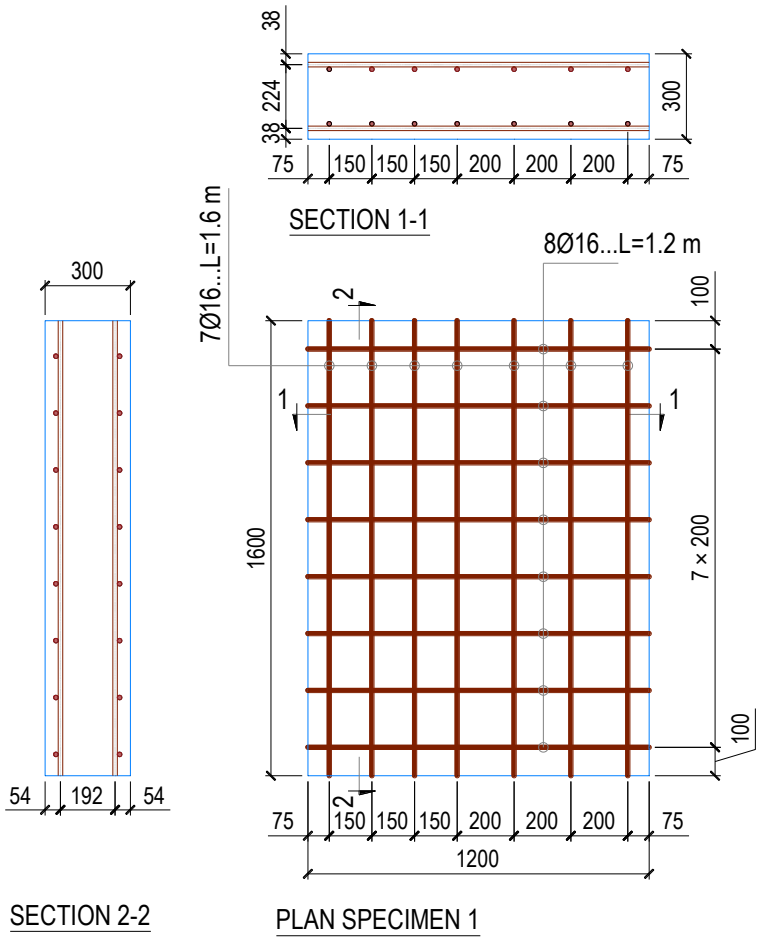

Figure 11 Design of specimen 1

The concrete used corresponds to C30/37, with specified values for compressive strength f_c, and modulus of elasticity E_c. Material samples were taken during casting to support destructive testing for cross-validation.

This specimen served two primary purposes:

1. **Verification of material properties** using non-destructive and destructive methods.
2. **Assessment of NDT performance** in locating embedded reinforcement, identifying bar diameters, and confirming layer positions.

In addition, the slab was used to evaluate the applicability of basic NDT instruments, such as the combined Schmidt hammer and ultrasonic pulse velocity method, for estimating in-situ concrete compressive strength.

The absence of ducts and defects made this specimen ideal as a reference slab, allowing evaluation of baseline measurement accuracy without interference from complex features. It also played a key role in distinguishing signal responses from intact rebar and concrete prior to introducing artificial defects in the remaining specimens.

3.1.2 Specimen 2

Specimen 2 was designed to introduce controlled complexity by simulating post-tensioned ducts with intentional voids. It shares the same outer geometry and reinforcement layout as Specimen 1—measuring 1600 × 1200 × 300 mm with Ø16 mm bars spaced at 100 mm and 200 mm on the top and bottom layers.

In this specimen, two vertical corrugated steel ducts were embedded: one half-filled with grout and one left intentionally ungrouted. The aim was to evaluate the detectability and differentiation of grouted versus ungrouted tendon ducts using NDT. The ducts were placed at a 150 mm depth from the top surface and symmetrically aligned across the width.

The positioning of the ducts under zones of both dense and sparse reinforcement allowed for testing how overlying rebar density affects signal quality and interpretation. As with Specimen 1, the concrete was of class C30/37. Tendons were inserted to mimic real-world bridge post-tensioning scenarios.

This configuration supports training and method validation focused on locating ducts, estimating grouting extent, and understanding how tendon visibility is influenced by rebar congestion. However, unlike more intricate configurations, the relatively simple layout ensures that each feature can be clearly linked to the corresponding response in the NDT data—supporting both clarity in results and transferability to field conditions.

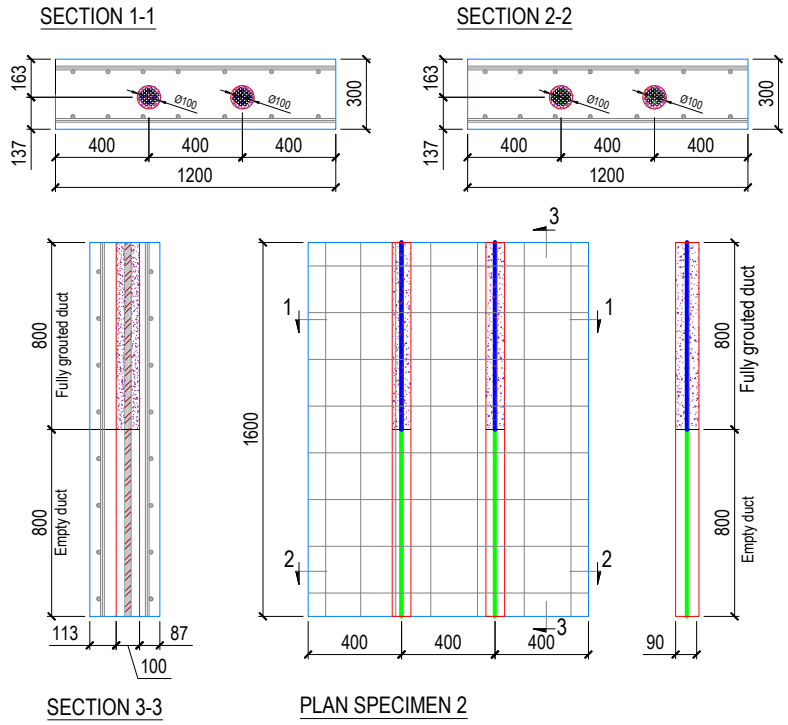

Figure 12 Design of specimen 2

3.1.3 Specimen 3

Specimen 3 is a 1600 × 1200 × 600 mm concrete slab, sharing the same reinforcement layout as Specimen 1, with top and bottom layers of Ø16 mm bars at 100/200 mm spacing. The specimen includes four vertical corrugated steel ducts embedded in two layers:

Top layer**:** Two ducts, each half fully grouted and half left empty (void).

Bottom layer**:** Two ducts, also alternating between grouted and empty segments, with the inverse pattern of the top layer to simulate alternating defect depth.

The vertical separation between layers is 170 mm, with the top ducts positioned 200 mm from the top surface and the bottom ones 200 mm from the bottom. Steel tendons were inserted in all ducts, consistent with post-tensioned bridge practice. The primary aim of this mock-up was to challenge NDT equipment and operators to:

- Locate tendons in both shallow and deep positions.
- Distinguish between fully grouted and voided segments within the same duct.
- Assess the influence of tendon depth and grouting pattern on NDT results.
- Investigate signal interference due to alternating voids across depth layers—an artificial but instructive complexity.

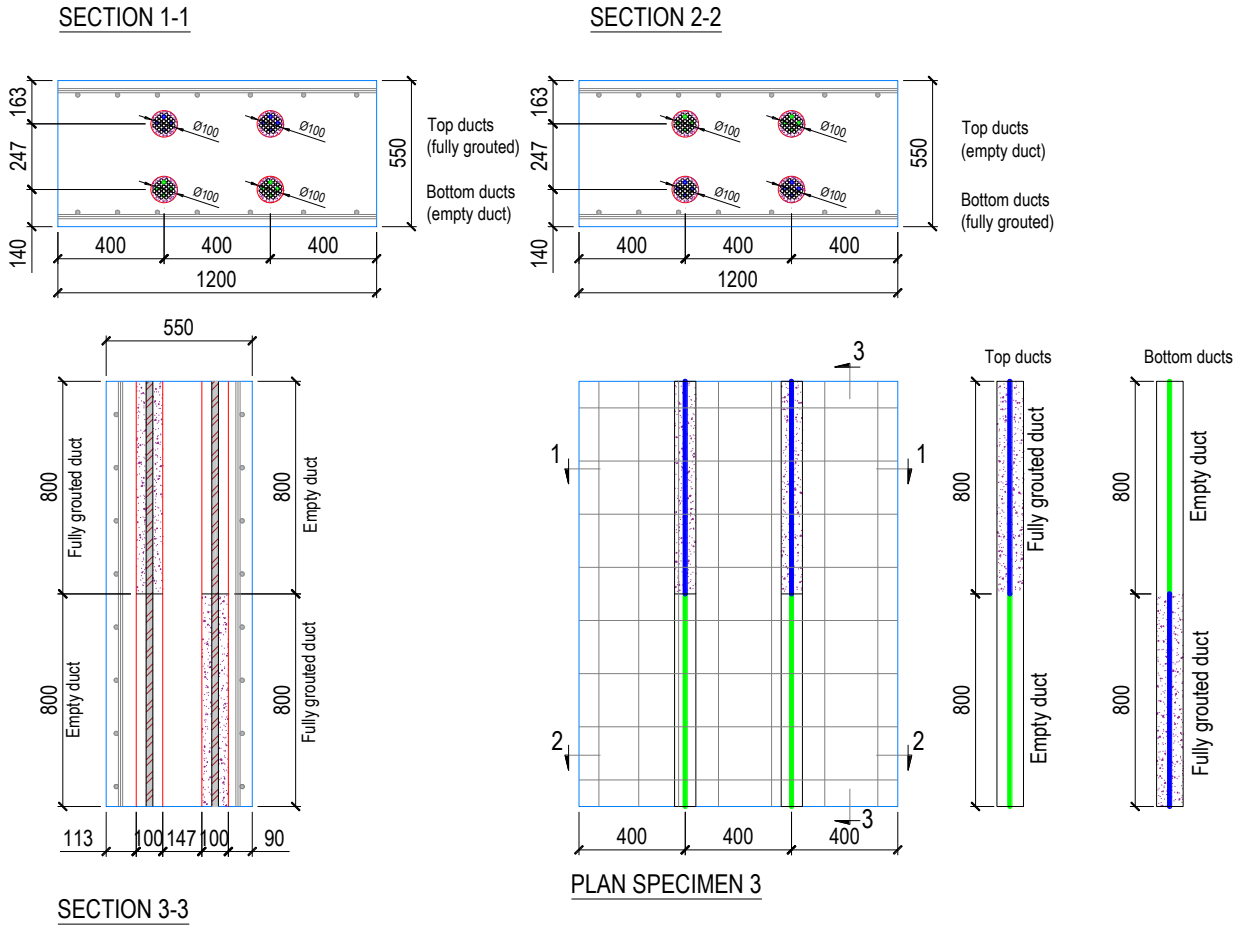

Figure 13 Design of specimen 3

3.1.4 Specimen 4

Specimen 4 was designed to simulate two common but distinctly different defect types often encountered in reinforced concrete structures: delamination and honeycombing. The specimen measures 1600 × 1200 × 600 mm and features the same reinforcement layout as Specimen 1, ensuring consistency in surface steel configuration across all mock-ups. No ducts or tendons were included, as the focus here was on material-related defects rather than tendon integrity.

To represent a delamination, a thin plastic foil (approximately 2–3 mm thick) was embedded horizontally below the top reinforcement layer, simulating a planar separation or poor bond between layers—something that may occur due to cold joints or improper casting. In addition to this, an irregular region of intentionally poorly compacted concrete was introduced near the bottom surface to mimic honeycombing, representing large internal voids caused by insufficient vibration or segregation during casting.

The purpose of this specimen was to evaluate how well NDT techniques can detect and differentiate between delaminations and volumetric defects such as honeycombs, particularly when they occur at different depths. It also served to challenge both the capabilities of the inspection equipment and the interpretative skills of operators.

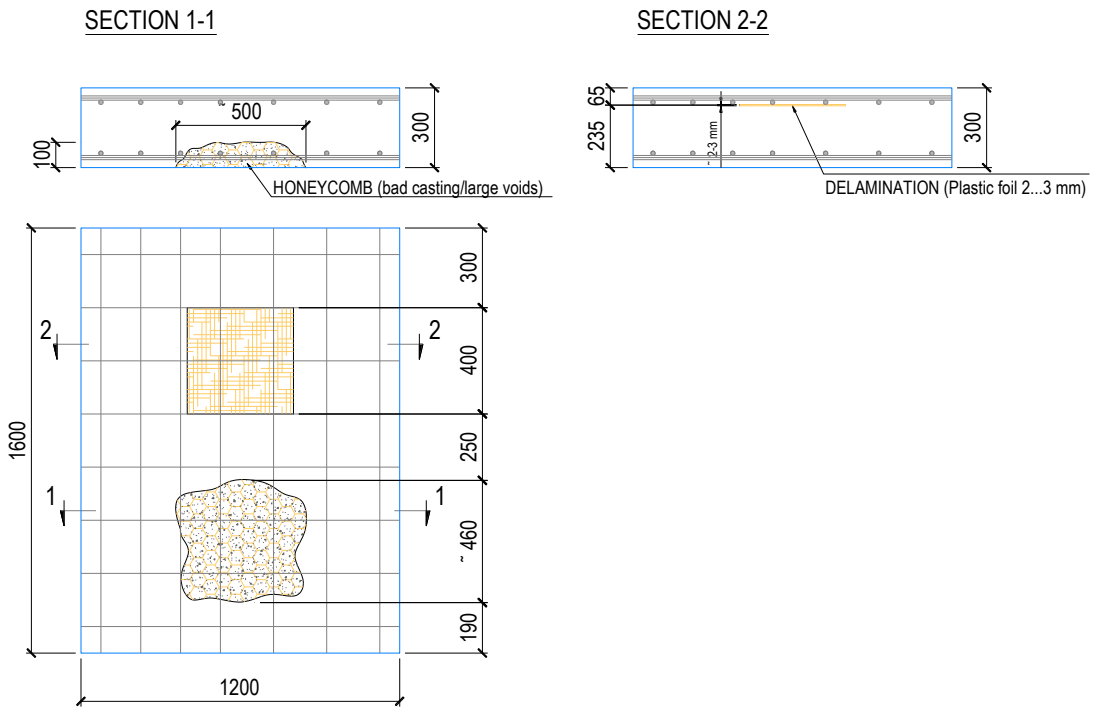

Figure 14 Design of specimen 4

3.2 Fabrication process of mock-up specimens

Before casting the final mock-up specimens, a prototype element was first constructed to test and refine the fabrication method. The aim of this prototype was to verify the feasibility of placing all reinforcement and artificial defects precisely according to the design drawings.

Given that each rebar had to be positioned with high accuracy to match the documented layout, the side edges of the formwork were specially modified. Custom protrusions were introduced along the inner face of the formwork walls to lock each bar into its correct position, thereby ensuring the intended concrete cover was achieved throughout the specimens.

The prototype phase also served to test several critical aspects of the process:

- The grouting procedure for tendon ducts, especially to simulate both fully filled and empty conditions.
- The installation of artificial defects, such as delamination foils and honeycombing areas.
- The handling sequence for integrating tendons, ducts, and reinforcement within the formwork.

Following successful validation, small adjustments were made based on the prototype outcomes, after which the fabrication of all four specimens commenced.

The production process included the following steps:

1. Pre-fabrication of artificial defects separately from the specimens.
2. Grouting of ducts (where applicable) before placing them into the formwork.
3. Installation of surface reinforcement and tendon ducts into the prepared formwork, using alignment guides and fixed spacers to maintain correct positioning.
4. Concrete casting, carried out after a final inspection of all embedded components to confirm compliance with the drawings and defect layout.

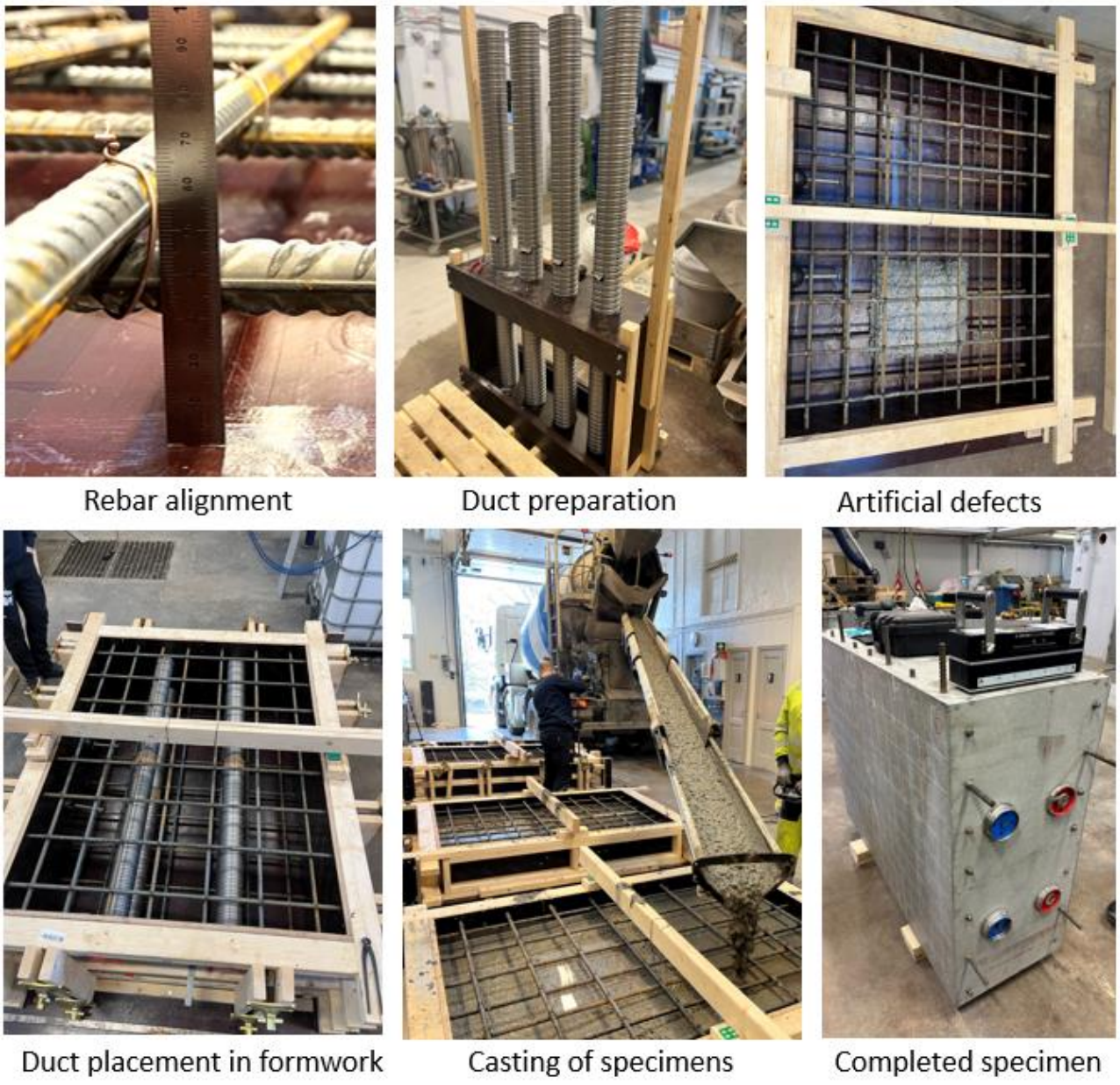

Figure 15 Fabrication process

3.3 Participating teams and testing objectives

Several teams participated in testing the mock-up specimens using their own equipment and methods. Each team had different goals depending on the technology they brought. The aim was to assess how well the defects could be detected and to explore the capabilities and limitations of various NDT techniques.

1. **SINTEF Narvik & Invator AB**

Aimed to detect all embedded defects using a combination of basic and advanced NDT methods:

- *Basic testing*: Schmidt hammer and ultrasonic pulse velocity (UPV)
- *Material properties*: Dry-coupled S-wave transducers for estimating dynamic E-modulus
- *Rebar and duct detection*: Cover meter and two types of GPR

- *Defect detection*: Ultrasonic tomography and impact-echo for locating voids, honeycombing, and delamination

2. **Elop AS**

Tested their proprietary ultrasonic roller scanner:

- *Purpose*: Detect internal concrete defects and voids in tendon ducts

3. **Equinor & Aker Solutions**

Focused on ultrasonic and GPR methods:

- *Ultrasonic pulse-echo*: For internal damage detection
- *GPR*: For locating rebar and tendon ducts

4. **Birdsview**

Conducted a limited test using a standard GPR system:

- *Purpose*: Identify reinforcement positions and estimate rebar diameter

3.3.1 NDT equipment and techniques

3.3.1.1 Ground-penetrating radar (GPR)

This method applies electromagnetic waves by moving one or two antennas over the concrete surface. It's important to note that if the variation in the dielectric properties of different materials is low, only a small amount of energy will be reflected. For example, electromagnetic waves cannot penetrate any metal layers. The shape of construction elements (e.g., rebar diameter) or material inhomogeneities is difficult or impossible to estimate. This method is often used to inspect the internal structure of building elements made of reinforced or prestressed concrete and masonry to detect and locate inhomogeneities (voids, metal or wood inclusions), thickness of structures that are only accessible from one side, the internal structure of complex elements, and in some cases, to determine moisture content and its distribution. GPR data are collected in either a 2D (distance and time) or 3D (x, y, and time) fashion, depending on the application.

Figure 16 provides an example of GPR usage. The evaluation of results heavily relies on existing algorithms and user interfaces. The possibilities and limitations of GPR inspection technology are discussed in Table 10, outlining GPR's capabilities and constraints.

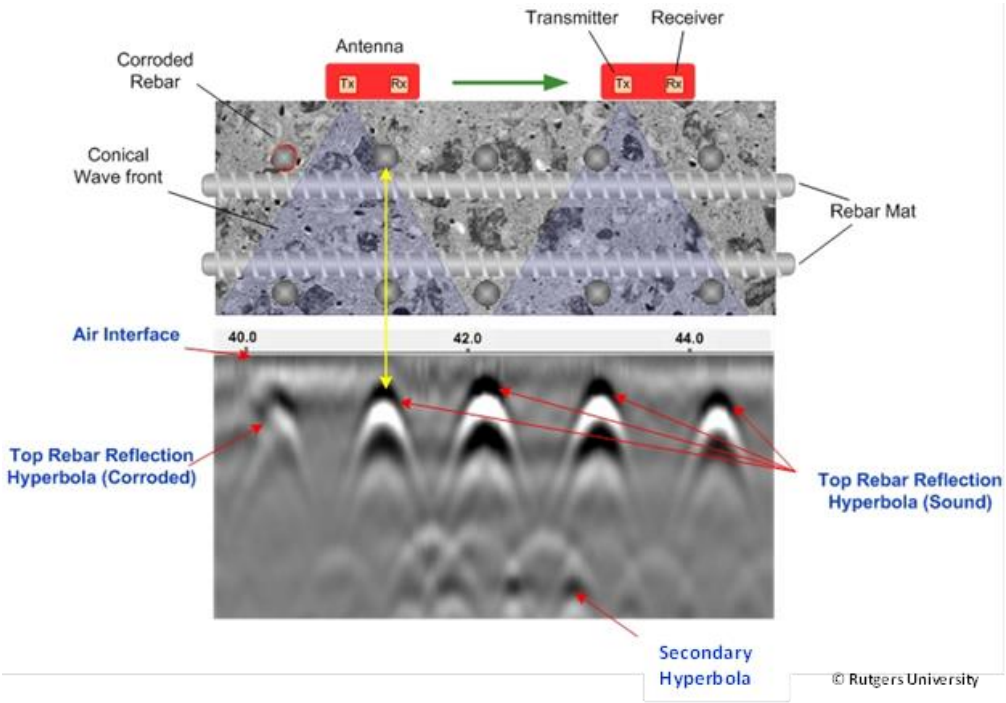

Figure 16: Ground-penetrating radar (GPR) (https://fhwaapps.fhwa.dot.gov)

3.3.1.2 Ultrasonic tomography (MIRA)

The specific type of wave used in ultrasonic testing can vary depending on the application and the equipment being used. Ultrasonic testing can employ both shear waves (also known as transverse waves) and pressure waves (also known as longitudinal waves).

- **Shear Waves (Transverse Waves):** Shear waves involve particle motion perpendicular to the direction of the wave. They are commonly used when the detection of flaws or the characterization of materials requires the analysis of shear wave reflections. Shear waves are especially useful for detecting flaws in concrete and examining the integrity of materials.
- **Pressure Waves (Longitudinal Waves):** Pressure waves involve particle motion parallel to the direction of the wave. They are often used for general ultrasonic thickness measurements and to detect flaws, voids, and other anomalies in a wide range of materials. Pressure waves are typically easier to generate and are widely used in industrial applications.

The choice between shear waves and pressure waves depends on the specific testing requirements and the nature of the material being examined. Each type of wave has its advantages and limitations, and the selection is made to optimize the inspection process for a given application.

An advanced ultrasound method is one often referred to as MIRA. However, MIRA is a trademark, and there is similar equipment that functions in a similar way, see, for example, (www.screeningeagle.com). The method is based on ultrasonic shear wave tomography. It relies on a low-frequency ultrasound system capable of detecting internal defects in reinforced concrete, such as voids and delamination. MIRA is based on the ultrasonic pitch-catch method and employs an antenna consisting of an array of dry point-contact transducers that emit shear waves into the concrete. An advantage of using MIRA is its scanning depth, which penetrates up to 1 m in heavily reinforced concrete structures and up to 2 m in lightly reinforced concrete structures. The control unit inside the antenna excites a row of transducers, and the other rows of transducers act as receivers.

Phase I in Figure 17b shows the first row of transducers functioning as transmitters, and the remaining rows of transducers functioning as receivers. Transition to the second row, where the receivers now act as transmitters, is depicted in Phase II. Here, the next row of transducers is excited, and the other rows to the right function as receivers. This process is repeated until each of the 10 rows of transducers has served as a transmitter, as seen in Figure 17 a) - c).

If there is a sufficiently large interface between concrete and air (a defect) inside the element, a portion of the emitted wave will be reflected by the defect, as illustrated in Figure 17c). MIRA equipment system is consists of a phase-controlled antenna system, a portable computer with MIRA software (the software is based on SAFT - Synthetic Aperture Focusing Technique), and a power unit. To perform a scan, the user lays out a series of parallel scan lines on the surface to be examined. The signals captured by the antenna are automatically transferred to the computer, where the SAFT algorithm is used to reconstruct a 3D model of the concrete's internal structure.

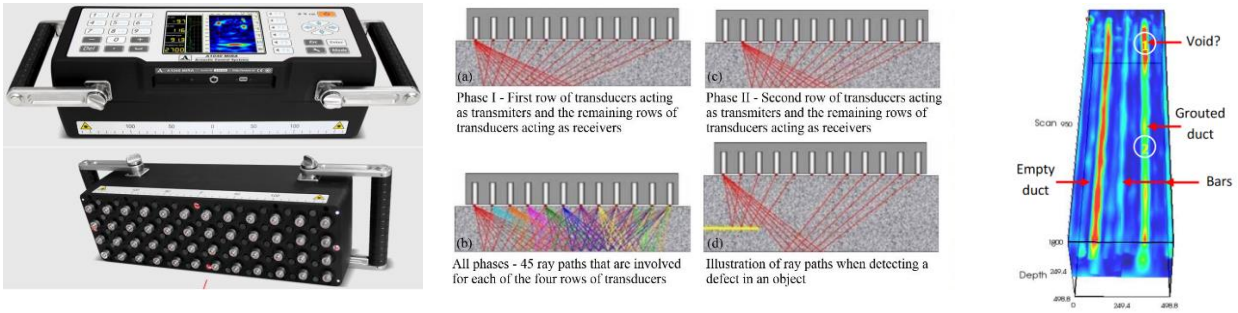

(a) (b) (c)

Figure 17: Shear wave tomography: (a) MIRA equipment; (b) working principle; and (c) MIRA 3D image grouted vs un-grouted tendon ducts (https://www.germanninstruments.com)

3.3.1.3 Ultrasonic tomography (Elop Insight)

An alternative approach to concrete imaging involves utilizing the Elop Insight Ultrasonic Scanner (Figure 18), which provides a dry coupling solution for detecting damage within concrete structures. The Elop Insight (EI) is a rolling ultrasonic scanner that employs all eight transmitters and eight receivers, offering up to 64 combinations akin to Full Matrix Capture (FMC) for cross-track synthetic aperture.

In the process of image reconstruction, Full Matrix Capture (FMC) is achieved when A-scans from all sensor element combinations within an array are utilized. Additionally, Total Focusing Method (TFM) is implemented by focusing these A-scans into each grid position within the imaged volume. To further enhance data acquisition, the scanner incorporates a built-in rotational encoder during movement, extending the captured matrix in the scan direction to acquire a significantly higher number of data points.

Both the along-track and cross-track data are subsequently focused into each image grid point, or voxel (the 3D equivalent of a pixel), following the TFM approach, ensuring that imaged features are sharp and focused from all orientations. For the EI scanner, approximately 10000 A-scans are typically employed to generate amplitude data for each voxel in the 3D image, particularly in what we refer to as "high accuracy mode." This mode employs a 2 mm along-track sampling distance, meaning a complete set of up to 64 A-scans is acquired for every 2 mm of rolling with the scanner. This considerably surpasses the capabilities of non-rolling devices.

It is important to note that the primary distinction between high accuracy and high-speed modes lies in the along-track sampling distance and, consequently, the number of A-scans combined within each voxel. In

high-speed mode, the scanner can be moved at speeds of up to approximately 1 m/s, equivalent to a normal walking pace.

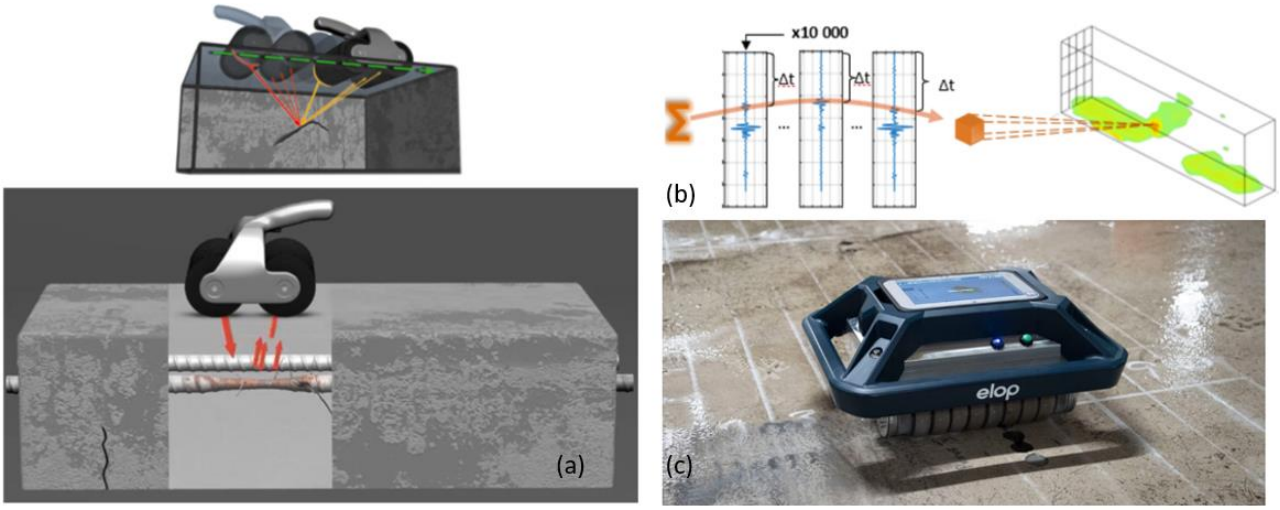

Figure 18: Elop Insight: (a) Ultrasonic signals sent and echoes received as the scanner moves; (b) SAFT delay-and-sum process; and (c) Elop Insight instrument (source: SAFT (Synthetic Aperture Focusing Technique) for 3D image reconstruction and noise reduction in Elop Insight Ultrasonic Scanner - Elop)

3.3.1.4 Ultrasonic Pulse Echo

The Ultrasonic Pulse Echo (UPE) equipment (Proceq PD8000 - Figure 19) is designed for non-destructive testing of concrete. The working principle is based on the reflection of ultrasonic waves within the material to detect internal features like voids, delamination, honeycombing, and thickness. An array of dry-point contact transducers (usually operating at ~50–100 kHz) generates a short, high-frequency ultrasonic pulse that enters the concrete surface. These are shear wave (S-wave) transducers, which are more sensitive to defects and propagate slower than pressure waves (P-waves), making interpretation easier in dense materials like concrete. The ultrasonic pulse travels through the concrete and reflects back when it encounters internal features like voids, delamination, or interfaces with different acoustic properties. These echoes are then captured by the receiver array, and the time it takes for the pulse to return is analyzed to determine the depth and location of the reflecting object. Advanced signal processing techniques convert this time-of-flight data into detailed 2D or 3D images, revealing the internal structure of the material.

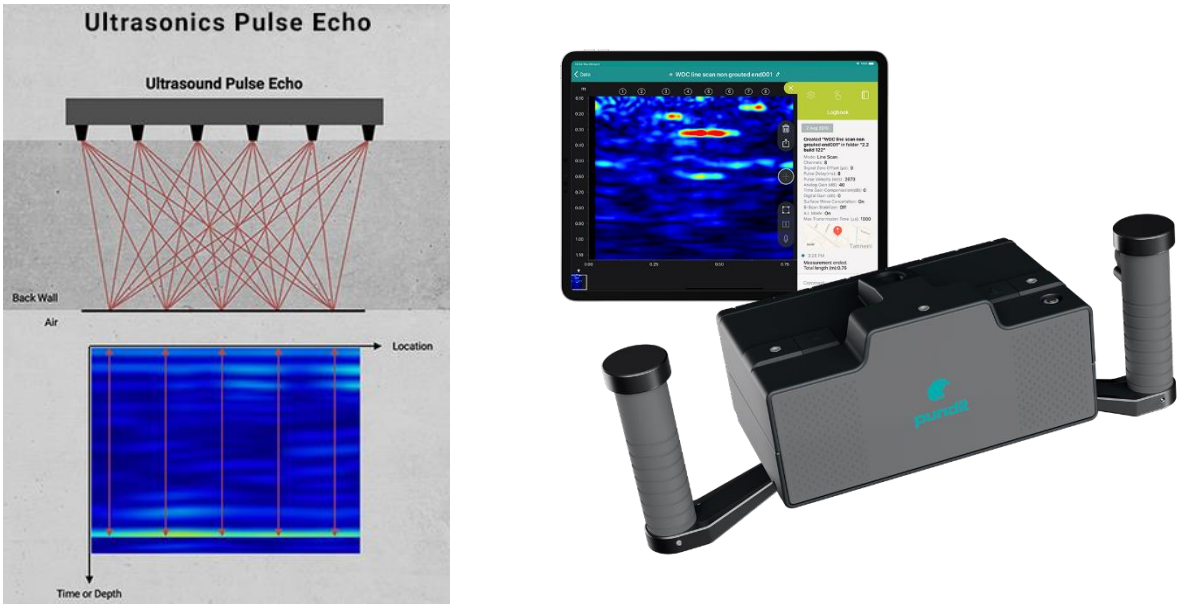

Figure 19: Ultrasonic Pulse Echo working principle and Proceq PD8000 (https://www.screeningeagle.com/en/products/pundit-pd8050)

4 Evaluation of NDT capabilities based on mock-up testing

4.1 Locating reinforcement and tendon ducts

Q1: Can the equipment detect surface reinforcement?
The ability to detect surface reinforcement was confirmed across all specimens using GPR. Both 2D line scans and grid-based area scans were performed. In the line scans, rebars appeared as characteristic hyperbolas, easily recognizable and consistent with the known layout – particularly in central areas. However, bars near the edges were occasionally missed, likely due to signal drop-off or limitations in probe proximity to the specimen boundaries.

By combining orthogonal scans in horizontal and vertical directions, the teams produced area visualizations that reconstructed the reinforcement mesh in plan view. This provided a clear overview of bar spacing and alignment across the scanned area. Area scans proved especially useful for intuitive interpretation in regions with dense reinforcement.

Two teams employed the Proceq GP8000 GPR system independently but used similar scanning approaches. Despite slight variations in scan quality – possibly due to operator technique or post-processing – both produced clear and reliable results (Figure 20). The mesh of longitudinal and transverse bars was consistently visible, confirming that GPR was effective and user-friendly for mapping surface reinforcement across all specimens.

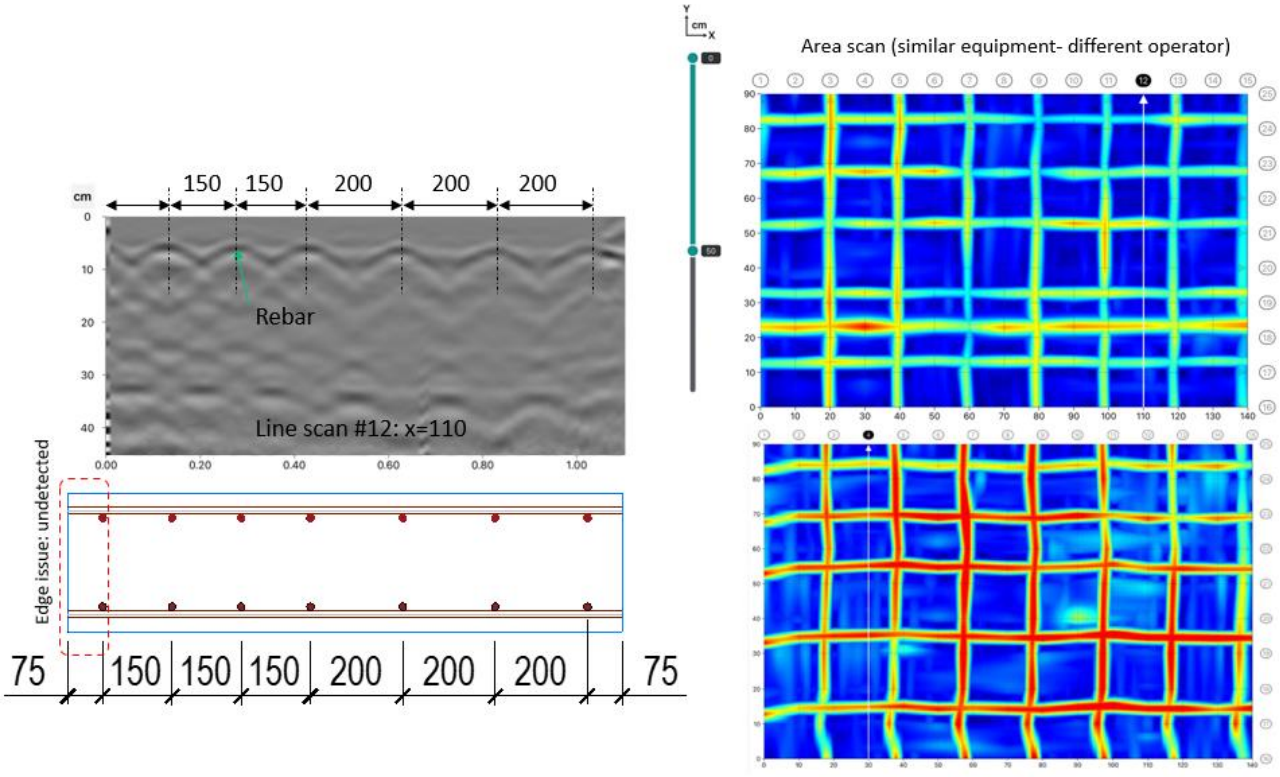

Figure 20. Surface reinforcement detection using the Proceq GP8000 GPR by two independent teams

Another team applied a rolling ultrasonic scanner with the aim of detecting surface reinforcement, despite this not being the primary use case of the equipment. The top transverse rebars were partially captured in the B-scan images, where reflections appeared at positions that aligned reasonably well with the known spacing. However, the reflections were relatively diffuse, and some bars, particularly those near the scan boundaries, were either poorly resolved or not visible.

Detection of the top longitudinal rebars proved more challenging. These bars could not be directly imaged in the standard B- or D-scans, likely due to their shallow depth – close to the surface – and the scanner's inherent limitations in that near-surface region. Instead, the approximate location of these bars was inferred indirectly by observing disruptions in near-surface wave propagation, particularly Rayleigh waves.

To enhance the visibility of the reinforcement, the team applied alternative processing techniques, including beamforming and time-gain compensation. C-scans generated with these algorithms offered a clearer view of the bar layout and showed reasonable agreement with the actual mesh geometry, although the signal remained smeared and the positioning less precise than with electromagnetic methods.

Overall, the ultrasonic approach demonstrated some potential to detect surface reinforcement, particularly with advanced post-processing. However, the results (Figure 21 and Figure 22) were weaker and less consistent compared to GPR-based scans, especially for shallow and small-diameter rebars.

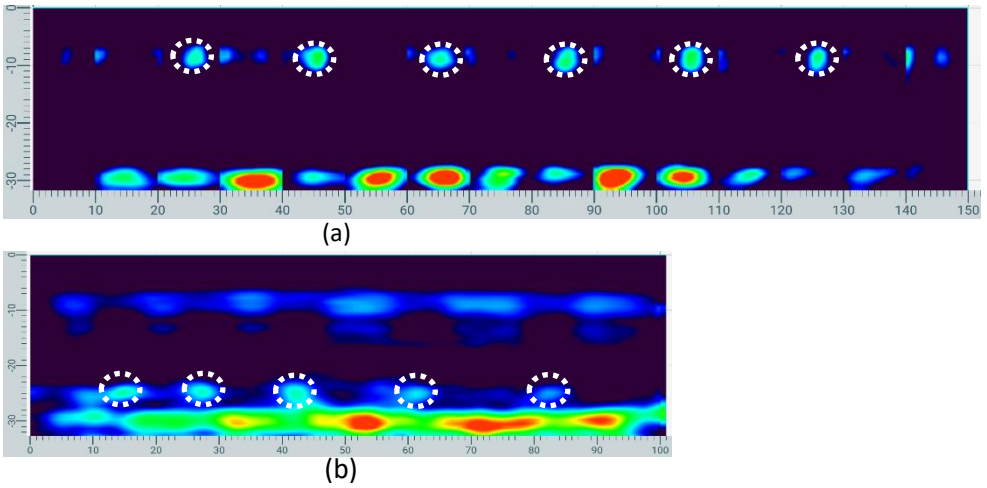

Figure 21. (a) B-scan showing reflections from the top transverse rebars, along with backwall echo at 30 cm depth. (b) D-scan showing weaker reflections from the bottom longitudinal rebars.

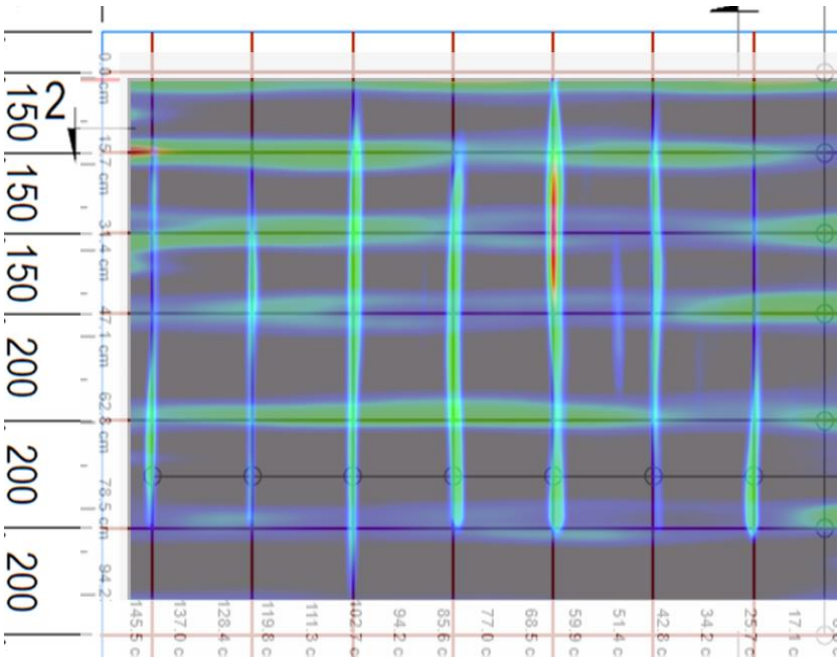

Figure 22. C-scans from the first reinforcement layer superimposed on the drawing for specimen 1.

One of the participating teams employed a GPR system (Proceq GP8800) enhanced with machine learning-based Full Waveform Inversion (FWI) algorithms to analyze surface reinforcement. The method produced a clear mesh visualization.

The rebar layout was mapped across the entire scanned area, with estimated spacings of 150 mm and 205 mm aligning well with the actual values of 150 mm and 200 mm – showing a maximum deviation of only +5 mm (Figure 23).

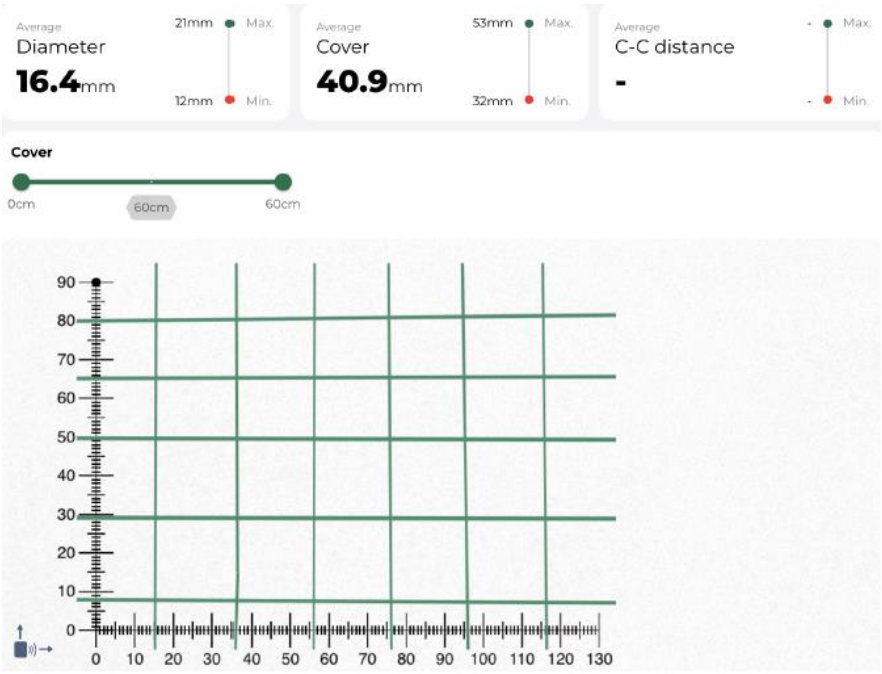

Figure 23. Automatically reconstructed rebar mesh based on GPR data processed with advanced signal interpretation algorithms

Q2: Can deeper ducts be located?

The ability to locate deeper-embedded post-tensioning ducts was successfully demonstrated using GPR, with multiple teams applying similar equipment (Proceq GP8000) but varying in their processing and visualization approaches. The ducts in question were embedded beneath the reinforcement mesh, at depths approaching 140 mm from the surface for the first layer of ducts and 360 mm for the second layer (see Specimen 3). In all cases, the GPR system detected the first layer of ducts with a high degree of clarity. One team relied on traditional 2D B-scans to identify the characteristic hyperbolic reflections. In addition to the B-scans, this team produced a 3D volumetric reconstruction combining multiple orthogonal scans. The resulting model clearly separated the duct layer from the overlying reinforcement, offering an intuitive view of the structural layout. A second team approached the task through a series of depth-sliced C-scans derived from the GPR data. These horizontal slices at selected depths highlighted the duct locations with high contrast, clearly showing their position and continuity. Despite the differences in visualization techniques, both teams achieved successful and consistent detection of the first layer of ducts (Figure 24).

Importantly, when assessing the presence of a second layer of ducts – deeper and closer to the backwall – the results were more ambiguous. In the 2D scans, reflections from the second layer were weak and difficult to distinguish confidently from background noise or signal interference.

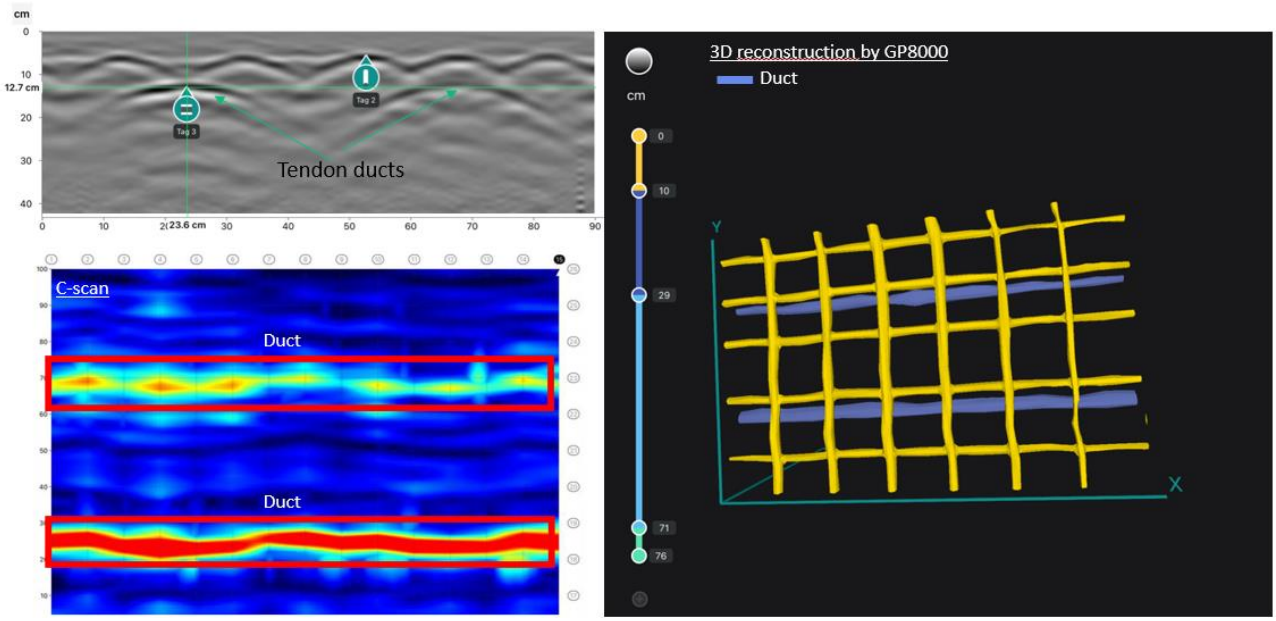

Figure 24. First layer duct detection (specimen 3) using the Proceq GP8000 GPR by two independent teams

Team 2 was able to indicate possible traces of this deeper layer in their C-scans, as highlighted in boxed regions, but the signal was faint and fragmented (Figure 25). This reduced clarity is not primarily due to the depth itself – since 360 mm is within the effective range of GPR – but rather the result of the duct geometry and alignment. The large duct diameters, combined with their vertical stacking and limited separation, created a shadowing effect where reflections from the upper layer obscured or interfered with signals from the lower ducts, making the second layer more difficult to interpret with confidence.

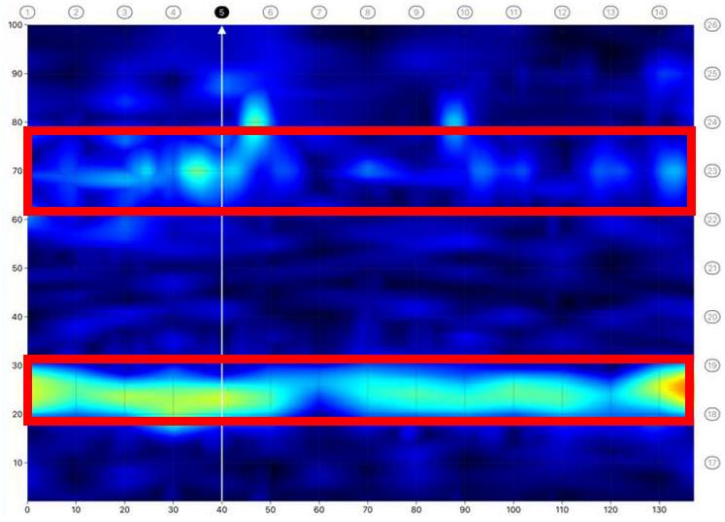

Figure 25. Attempt to detect the second layer of ducts in Specimen 3 using a C-scan from the GP8000.

The final team employed the GP8800 GPR system enhanced with machine learning algorithms show successful detection and visualization of the first layer of tendon ducts (Figure 26). However, the second layer of tendon ducts was not identified in the output.

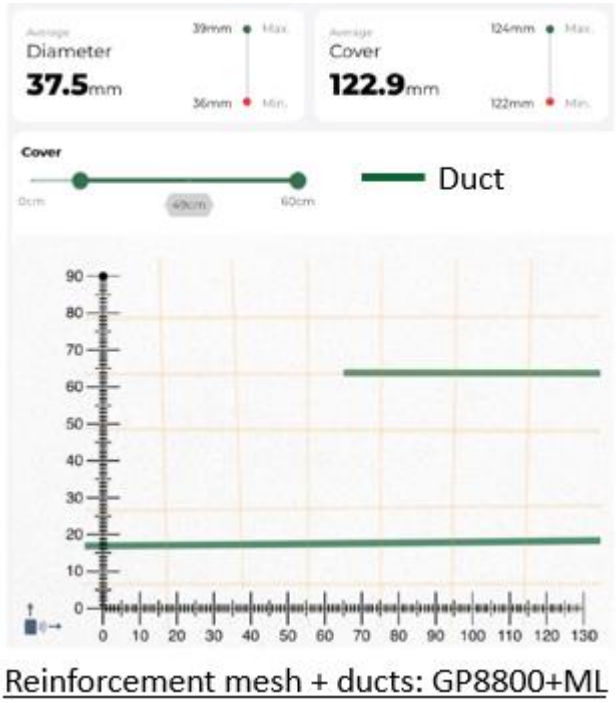

Figure 26. Automatically reconstructed rebar mesh + tendon ducts based on GPR 8800 data processed with advanced signal interpretation algorithms

Q3: Can the concrete cover (depth to reinforcement or duct) be estimated accurately?
Overall, most teams were able to estimate the concrete cover with good accuracy, especially for the top reinforcement layers. For instance, one team reported average cover values of 33.4 mm and 51.7 mm for the two orthogonal reinforcement directions, which aligns well with the true values of 38 mm and 54 mm, respectively. Of greater relevance, however, is the ability to determine the depth to the embedded tendon ducts. Reported values from two teams using similar GPR equipment (GP8000) but operated independently were 127 mm and 150 mm, compared to the as-designed depth of 140 mm. Additionally, a separate estimation using the GP8800 system combined with machine learning techniques yielded a predicted duct cover of 122.5 mm. These results demonstrate reasonable consistency across both equipment types and operators, with variations remaining within acceptable bounds for field assessment purposes.

Q4: Can the diameter of reinforcement or ducts be estimated?

In general, estimating reinforcement or duct diameter directly from raw GPR output remains unreliable. Most commercial GPR systems are not inherently designed for accurate diameter quantification, particularly when relying solely on amplitude or reflection pattern interpretation. However, one team extended the capabilities of the GP8800 unit by incorporating machine learning (ML) algorithms to estimate diameters. For standard reinforcement (Ø16 mm), the ML-enhanced system produced an estimate of 16.3 mm. For a tendon duct with a true diameter of 100 mm, the system returned a significantly underestimated value of 37.5 mm (Figure 26). This discrepancy highlights the limitations of existing algorithms, which are typically optimized for smaller-scale objects like rebars. Therefore, while ML techniques show promise in enhancing diameter estimation, the reliability currently appears limited to conventional reinforcement sizes within the trained parameter range.

Q5: Is there a visible difference between a tendon duct and a large rebar?
Distinguishing between tendon ducts and large-diameter rebars in GPR data is not always straightforward and depends significantly on the spatial arrangement, depth, and post-processing capability. In the B-scan image, tendon ducts manifest as pronounced hyperbolic reflections, and in this specific case, their apex depth is noted around 12.7 cm (Figure 24). While these hyperbolas appear more extensive than those typically generated by single rebars, their shape and amplitude can be influenced by multiple factors, such as nearby reinforcement, signal attenuation, and material heterogeneity.

Interpretation bias may occur, especially when one has prior knowledge of the geometry, as was the case in this exercise. Without this prior information, in field conditions, the presence of large-diameter rebars placed close to ducts could lead to overlapping reflections, making it challenging to differentiate between the two solely based on the B-scan.

One promising technique for improving distinction between ducts and rebars is the use of ML to estimate object diameter. Preliminary results show that ML-based analysis of GPR data can estimate rebar diameters with reasonable accuracy. While this approach is not yet robust enough for routine use, it suggests a potential path forward.

4.2 Detecting voids inside tendon ducts

Q6: Once the duct path is marked, can voids inside be detected? How is a "full" vs. "empty" duct visualized?

One team employed the Mira device, a synthetic aperture ultrasonic tomography system, to evaluate grouting condition inside the tendon ducts (Figure 27). Following duct path identification using GPR and physical marking on the concrete surface, Mira scans were conducted at intervals of 10 cm along each tendon. The recorded B-scans were post-processed to construct a 3D C-scan volume, allowing clear interpretation at the duct depth. In the resulting image, filled and empty duct segments are distinctly identifiable based on the intensity distribution at the duct level and, more importantly, the presence or absence of a back-wall reflection at 300 mm depth (i.e., the specimen thickness).

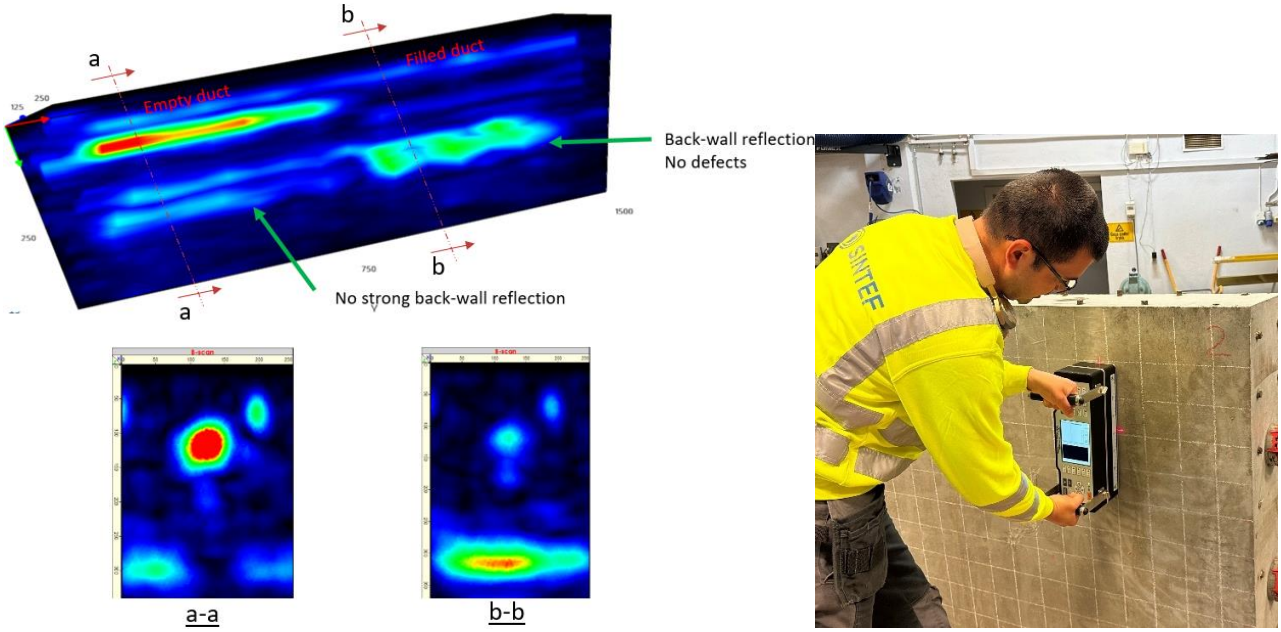

Figure 27. Mira scanning along tendon duct showing void vs grouted duct.

Where the duct is fully grouted, the ultrasound signal passes through with minimal attenuation, resulting in a strong back-wall reflection – interpreted as “no defect.” Conversely, in sections where the duct is ungrouted or voided, signal reflections are scattered or absorbed at the duct level, producing a significantly weaker or missing back-wall signal. This attenuation corresponds spatially with the duct depth, confirming the presence of a void. This combined depth-specific attenuation and back-wall reflection analysis proved effective in detecting ungrouted sections along the duct length.

The results were further verified using Impact-Echo testing (Figure 28). The Impact-Echo method evaluates the dynamic response of concrete by introducing a mechanical impact and analyzing the reflected stress waves in the frequency domain. In the filled duct, the impact generates a relatively continuous medium for wave transmission. As a result, the frequency spectrum shows a stronger and sharper peak. In contrast, the empty duct acts as a major acoustic impedance discontinuity. When stress waves reach the void (air or ungrouted section), a large portion of the wave energy is reflected back prematurely. This results in:

- A broader and lower-amplitude frequency spectrum, due to the wave energy being scattered or absorbed at the duct location rather than traveling to the back wall
- A shift in dominant frequencies and a generally weaker or absent backwall echo, as the wave energy does not reach the full thickness of the concrete

This contrast between the two conditions is evident in the comparison of the measured and calibrated frequency spectra: the filled duct spectrum shows well-defined resonant peaks, while the empty duct spectrum appears damped and irregular.

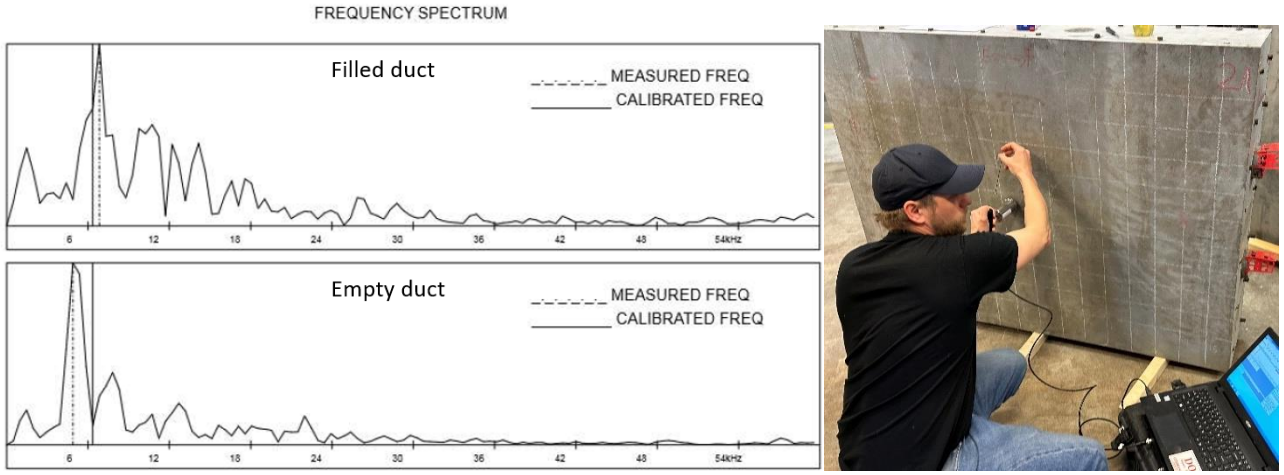

Figure 28. Impact-Echo frequency spectra showing a clear peak for the filled duct and a damped response for the empty duct, indicating internal void presence

Pulse Echo device (Proceq) was used to scan the side face of a concrete element known to contain two tendon ducts (the first layer). The resulting image (Figure 29) overlays a color map onto the physical surface of the specimen, where the intensity of colors corresponds to the amplitude of reflected ultrasonic signals. The goal was to evaluate whether differences in duct grouting condition (filled vs. ungrouted) could be inferred from the color distribution alone. While both ducts are visible in the scan, the reflections appear diffuse and lack sharp contrast, making it difficult to confidently differentiate between filled and empty ducts based solely on the visual intensity pattern. Although, in theory, ungrouted ducts should generate stronger reflections due to impedance contrast, in practice, interpretation remains challenging without prior knowledge or confirmation from another method. Thus, distinguishing between filled and unfilled ducts using only the Pulse Echo color map would require either strong operator experience or additional supporting data, underscoring the need for multi-method approaches or validation through techniques like Impact Echo or ultrasonic tomography.

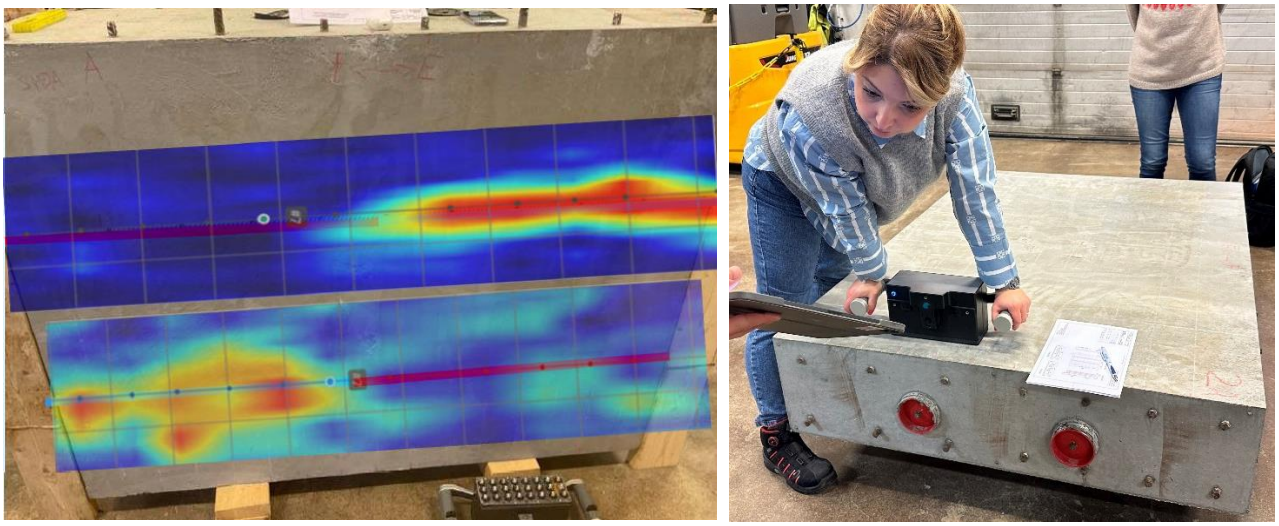

Figure 29. Pulse Echo (Proceq) scan on the side face of the specimen

Finally, the Elop Insight team employed a roller-based ultrasonic system to inspect the ducts for voids (Figure 30). Three scanning approaches were tested: (1) area scan crossing the ducts, (2) area scan parallel to the ducts, and (3) single-line scan along the duct path. All methods successfully identified the empty portions of the ducts, which produced significantly stronger direct reflections in the C-scan images. In contrast, the grouted sections typically resulted in lower signal amplitudes, often falling below the amplitude threshold and thus appearing faint or absent in the scans. The results also demonstrated that voids could be inferred through changes in the backwall reflection. Specifically, the empty segments of the ducts created shadow zones at the backwall due to nearly complete signal reflection at the concrete–air interface. Conversely, the grouted portions allowed partial transmission through the duct material, preserving the visibility of the backwall echo. Among the three scanning strategies, all showed comparable results in terms of void detectability. However, method 2 (parallel scan - Figure 31) appeared slightly clearer in image quality, while method 1 (cross-scan - Figure 30) offered strong signal-to-noise ratio and coverage. Method 3 (single-line scan - Figure 32) proved to be an efficient approach when duct positions were known in advance and accurately marked, offering high-quality results with improved time efficiency.

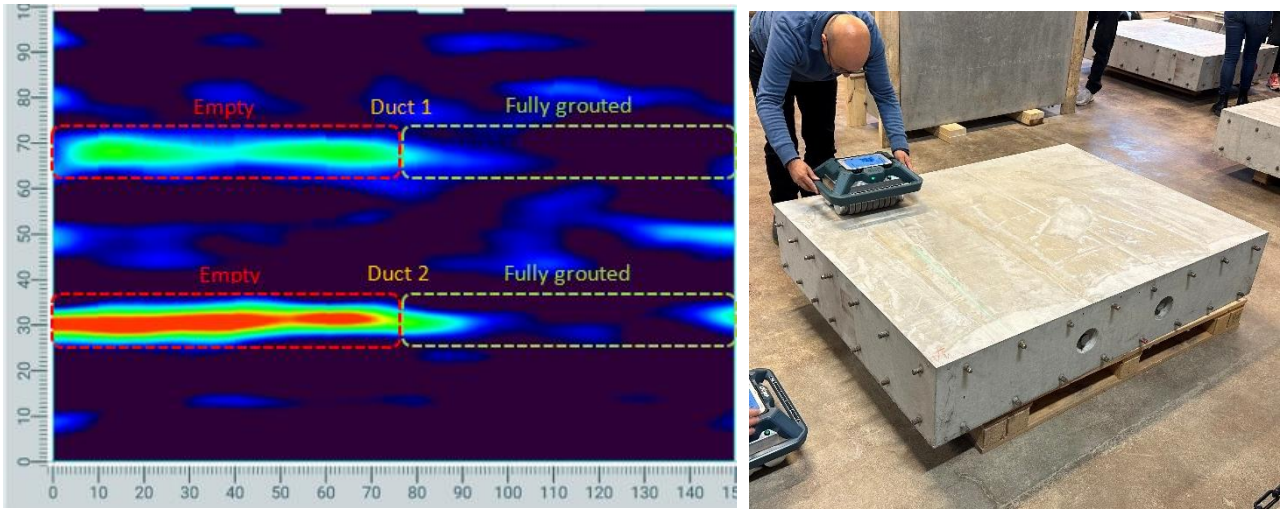

Figure 30. Elop Inshight - Method 1, area scan crossing the ducts

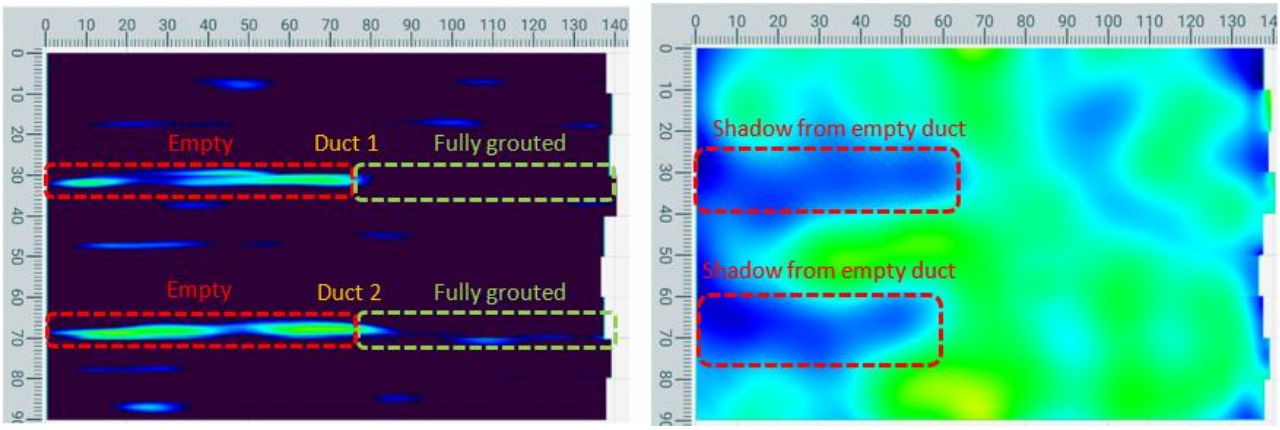

Figure 31. Elop Inshight - Method 2, area scan parallel to the ducts

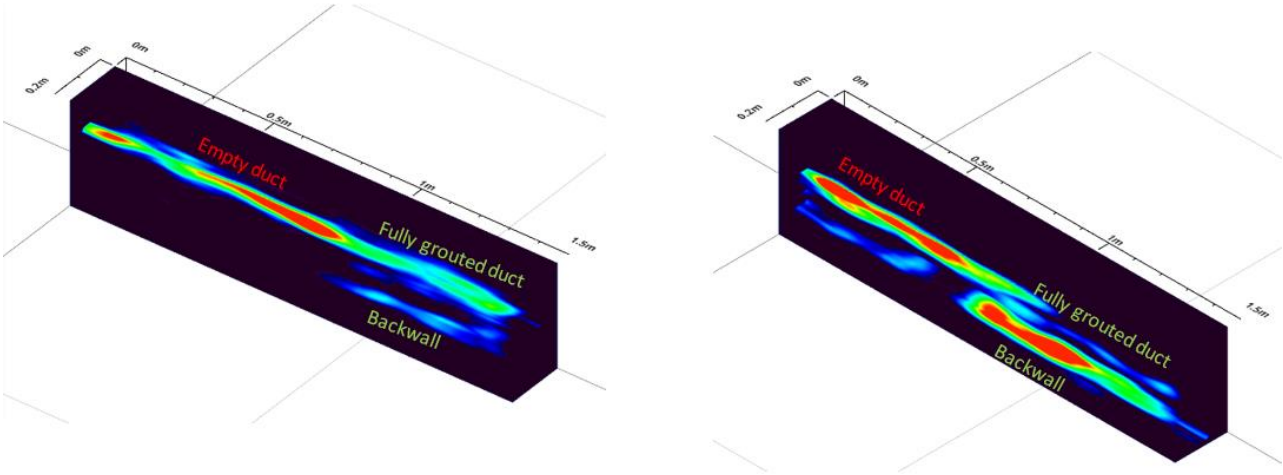

Figure 32. Elop Inshight - Method 3, single scan following the ducts

Q7: Can voids be detected when ducts are arranged in multiple layers

One team, using the MIRA ultrasonic tomography system, attempted to detect voids in the second duct layer positioned behind a full duct in the first layer. As shown in Figure 33, while the first (outermost) layer was successfully imaged – clearly distinguishing between filled and empty segments – there was no clear indication of voids in the second, deeper duct layer. The absence of strong reflections or back-wall signatures suggests that wave interference and shadowing from the first layer likely hindered detection. This highlights the limitations of current tomography approaches in resolving features behind complex or layered ducts.

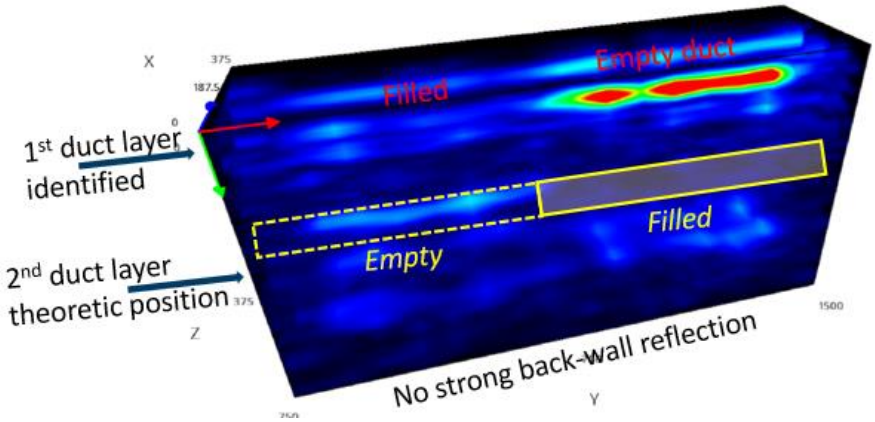

Figure 33. Mira scan performed along the duct axis in an attempt to detect voids within the second layer of tendon ducts

The roller-based ultrasonic scanner's ability to detect grouting defects (voids) in a more challenging setup, e.g. Specimen 3 was also employed.

The scanning was performed first from front side of the specimen (Figure 34). The team presented C-scan images at three depth intervals: the depth of the first (front) duct layer, the second (obstructed) duct layer, and the backwall of the specimen. For the first duct layer, the results were clear and consistent – the scanner was able to distinguish between the filled and empty sections, with the empty regions producing significantly higher amplitude reflections. This result was repeated and confirmed when scanning was performed from the backside of the specimen (Figure 35). At the depth of the second duct layer, which lies behind the first, the situation was more complex. The scanner was still able to capture some fragmented high-amplitude reflections in locations corresponding to the empty regions, suggesting that ultrasound waves did manage to partially penetrate the filled first layer and reflect off the voids behind it. However, these reflections were less clear. This made interpretation more uncertain and indicated the limits of detectability under such conditions. Finally, C-scans taken at the backwall depth showed clear shadowing effects across the length of the ducts. In particular, when voids were present in either duct layer, the ultrasonic signals were almost entirely blocked, resulting in a distinct absence of backwall reflection. This indirect evidence was used by the team to support the presence of voids, even when direct imaging was inconclusive (Figure 36). These results reflect both the potential and the current limitations of one-sided ultrasonic scanning in congested structural conditions.

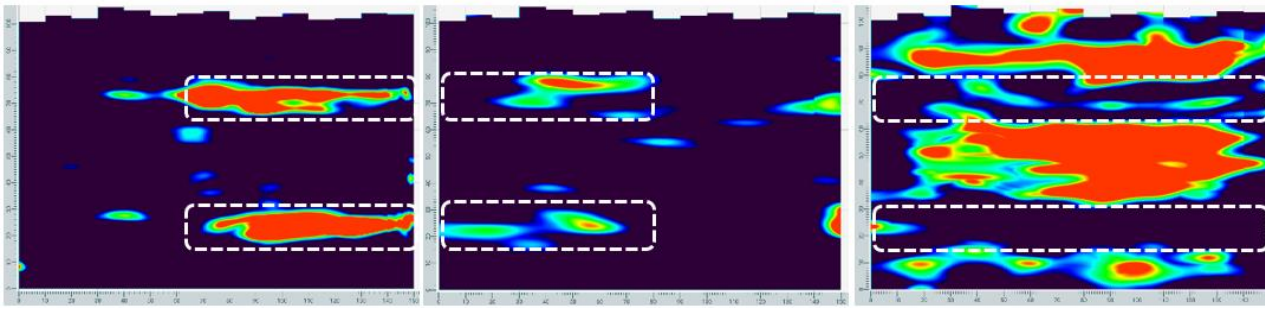

First duct layer Second duct layer Backwall

Figure 34. Elop insight C-scans from Specimen 3 frontside

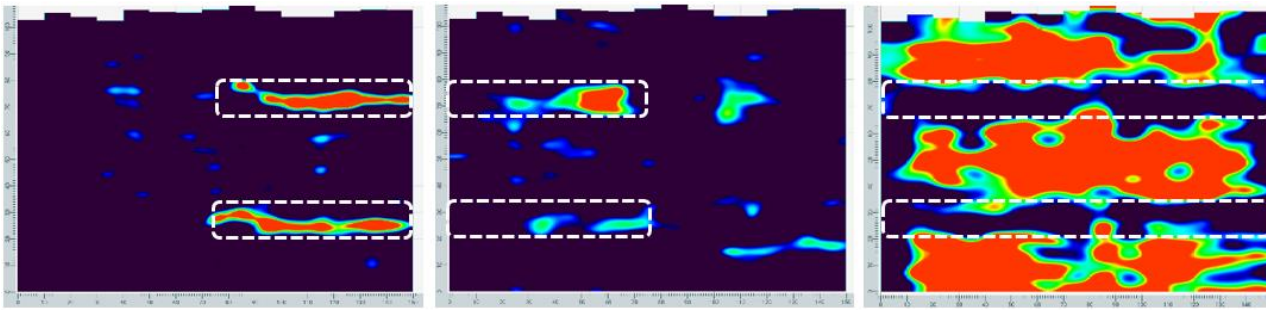

First duct layer Second duct layer Backwall

Figure 35. Elop insight C-scans from Specimen 3 backside

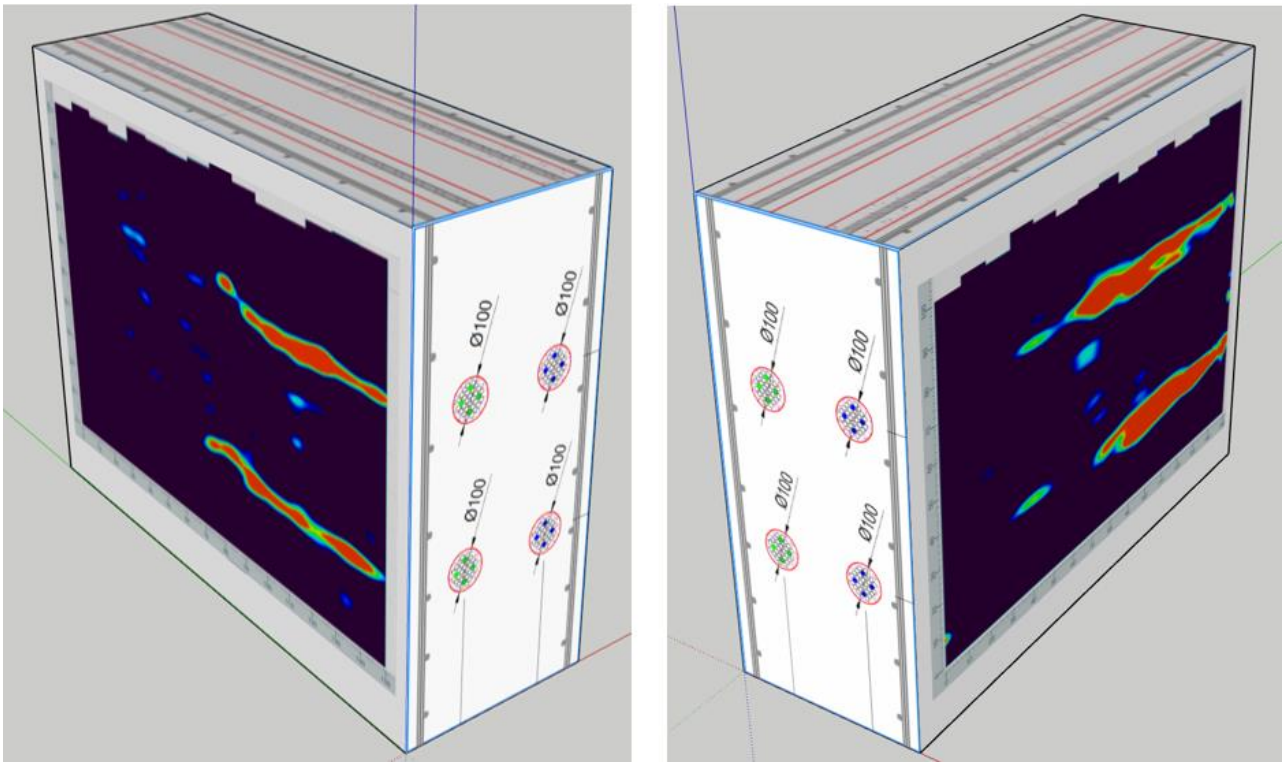

Figure 36. C-scans of the first layer of tendon ducts obtained from both faces of Specimen 3, superimposed on a rectangular block model along with the reference drawings

4.3 Detecting delamination and honeycombing

Q8: Can internal defects such as delamination and honeycombing be detected and their extent evaluated?

Figure 37 shows two C-scan slices taken at different depths from a MIRA area scan. The left image corresponds to a deeper slice closer to the bottom surface, revealing two prominent anomalies: one interpreted as a delamination and the other as a honeycomb defect. These areas appear as strong, localized reflections (in red), characteristic of air-filled or poorly compacted regions in the concrete.

The right image represents a shallower slice closer to the top surface of the specimen. Here, the same regions show weaker but spatially consistent reflections, particularly above the delamination zone, suggesting the defect extends vertically and is traceable through the depth slices. These results demonstrate that MIRA, operated in area scan mode, can capture reflections at multiple depths, allowing

defects such as delaminations and honeycombing to be localized and distinguished based on their vertical position and signal amplitude.

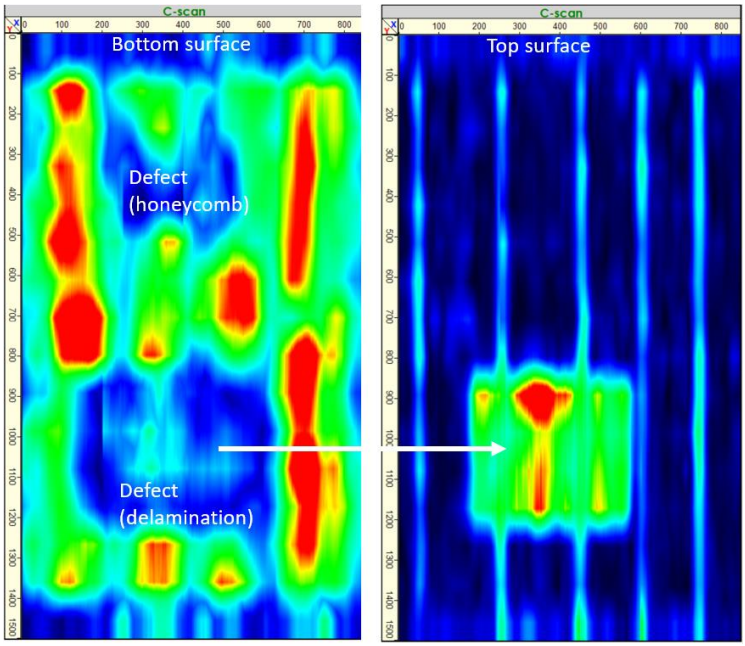

Figure 37. MIRA scans showing delamination/honeycombing inside Specimen 4

Based on the results presented in Figure 38, the ultrasonic roller successfully detected internal defects including delamination and honeycombing. A C-scan taken at a depth of 10–15 cm using a center frequency of 100 kHz revealed a clear and distinct reflection from a delaminated area approximately 40 × 40 cm, closely matching the known defect location. While honeycombing was not as clearly distinguishable through direct reflections – likely due to general scattering from large aggregates – it was nonetheless detected through characteristic shadowing observed in the backwall echo at 30 cm depth. This shadowing, visible even more distinctly in a scan using a higher 150 kHz frequency, aligns with both the delaminated and honeycombed regions. Thus, even when direct imaging is inconclusive, backwall shadowing can serve as a reliable indicator for evaluating the extent of internal damage such as delamination and honeycombing.

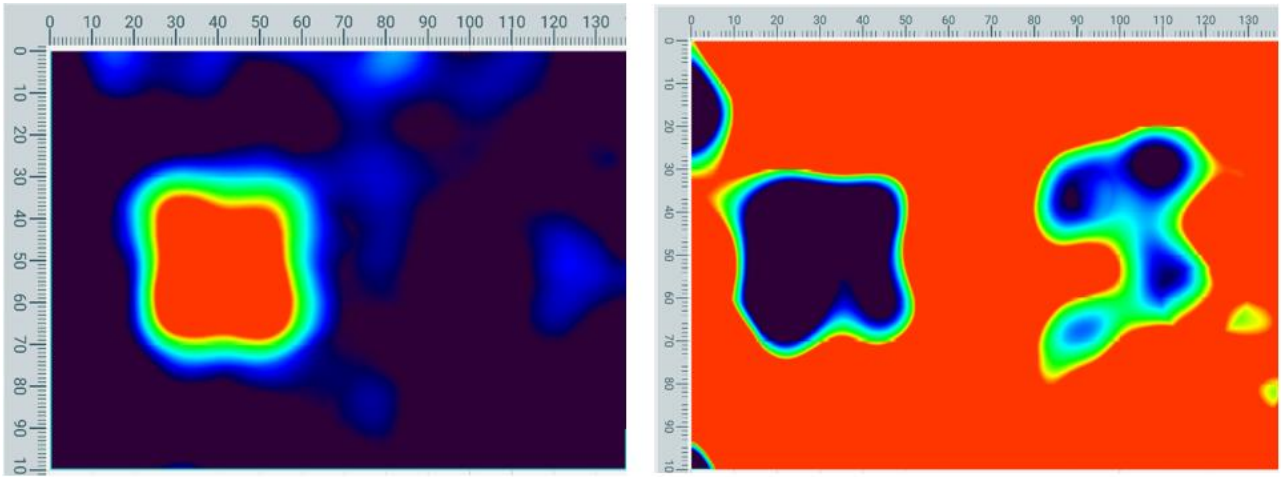

Figure 38. Elop Insight scans showing delamination/honeycombing inside Specimen 4

5 Discussion

The mock-up testing conducted in this project provides a controlled basis for evaluating the capabilities and limitations of selected NDT methods for detecting voids in tendon ducts of post-tensioned concrete structures. Unlike field inspections, where the internal condition of the ducts is largely unknown, the use of specimens with documented ground truth enables a more objective assessment of detection reliability, interpretation uncertainty, and method complementarity. The discussion below synthesizes the key insights gained from the experimental campaign and places them in the context of practical structural assessment.

The reliability of NDT for detecting voids in post-tensioned tendon ducts is governed not only by the technical capabilities of the equipment, but to a large extent by the competence and experience of the operator. Even when using identical hardware and software, inspection outcomes may vary significantly due to differences in scanning strategy, signal interpretation, and judgment under field constraints. This dependency becomes increasingly critical in complex geometries and under limited-access conditions typical of post-tensioned bridge structures.

The results confirm that tendon ducts can be reliably located using ground-penetrating radar (GPR), even in the presence of dense reinforcement, provided that scanning is performed systematically and with sufficient spatial coverage. GPR proved effective as a navigation and mapping tool, allowing reconstruction of duct alignment and depth, which is a prerequisite for the targeted application of ultrasonic methods.

Ultrasonic methods demonstrated a clear sensitivity to anomalies within or adjacent to tendon ducts. Fully ungrouted duct sections produced strong and repeatable reflections, particularly when the duct was located within a favorable depth range and not excessively shielded by reinforcement. However, specimens with multiple duct layers illustrated how signal interference and shadowing can complicate interpretation. In configurations where voided and grouted ducts were positioned vertically above one another, reflections from the shallower duct often dominated the response, making it difficult to assess the condition of deeper ducts independently. While such configurations represent deliberately challenging scenarios, they reflect real conditions encountered in multi-tendon bridge sections.

The mock-up results further illustrate that the absence of detected anomalies does not necessarily imply fully grouted ducts, particularly in deep or congested zones. Moreover, the findings highlight that confidently classifying the nature of detected anomalies—such as distinguishing between fully voided ducts, partially grouted ducts, or poor-quality grout—remains challenging. In many cases, NDT provides strong indications of irregularity without allowing unambiguous categorization of defect type.

The experimental campaign reinforces the importance of combining complementary NDT methods rather than relying on a single technique. GPR provides spatial orientation and duct mapping, ultrasonic tomography and pulse echo enable anomaly detection, and impact echo can assist in narrowing down areas of interest. Equally important is the sequencing of methods. The results demonstrate that ultrasonic testing is most effective when guided by prior knowledge of duct location and depth. Applying focused ultrasonic inspections without reliable duct mapping increases the risk of irrelevant measurements or misaligned interpretations.

Despite controlled conditions and known ground truth, interpretation uncertainty remained a recurring theme throughout the testing. Operator experience, familiarity with specific equipment, and prior exposure to verified defect scenarios strongly influenced interpretation outcomes. In field conditions, where access is limited and verification opportunities are scarce, this variability is likely to increase. These findings underline the importance of avoiding overconfident conclusions based on marginal or ambiguous signals. Where uncertainty cannot be reduced through complementary methods or targeted verification, it should be explicitly communicated rather than implicitly resolved.

From a structural assessment perspective, the results confirm that NDT-based void detection provides valuable but incomplete information. The presence of voids indicates a potential durability and robustness concern, but NDT alone cannot quantify corrosion state, residual prestress, or load-bearing capacity. Consequently, NDT findings should be interpreted as part of a broader assessment framework that includes structural analysis, historical documentation, and, where justified, targeted invasive verification.

6 Conclusions and Recommendations

The mock-up testing demonstrates that NDT methods can reliably locate tendon ducts and detect the presence of anomalies associated with voids in post-tensioned concrete structures under favorable conditions. Ground-penetrating radar is effective for duct localization and depth estimation and is a necessary prerequisite for targeted ultrasonic inspection. Ultrasonic methods are sensitive to ungrouted duct sections and other internal anomalies, particularly when ducts are located at moderate depths and are not heavily shielded by reinforcement. However, detection capability decreases with increasing depth, reinforcement congestion, and multi-layer duct configurations.

NDT inspections of post-tensioned tendon ducts should be based on a structured, multi-step workflow rather than single-technique application. Thus, the primary outcome of this work is therefore not a single "best method," but the establishment of a verified and repeatable testing environment in which NDT performance, workflows, and interpretation can be evaluated against known conditions.

The results show that the reliability of NDT in post-tensioned structures is governed as much by workflow discipline and operator competence as by equipment capability. To reduce variability and avoid systematic underestimation of risk, training must extend beyond laboratory demonstrations. A staged competence model is recommended:

- **Laboratory-based calibration** using mock-up specimens with known ground truth to align interpretation across inspectors and organizations.
- **Field-based verification**, where selected inspection findings are confirmed under real bridge conditions to expose access limitations, eccentric tendon positions, and practical constraints.

The mock-up specimens developed in this project provide a strong foundation for a national test bed for inspection of post-tensioned concrete structures. Future expansion of the test bed should include more realistic void configurations reflecting conditions observed in existing post-tensioned bridges including partial grouting, moisture-filled zones, and irregular void shapes.

To fully integrate NDT-based void detection into bridge management practice, further work is required in the following areas:

- Quantifying detection reliability, so that inspection results can be expressed with known confidence levels and used in risk-based assessments.
- Linking NDT findings to engineering decisions, including inspection intervals, need for verification, monitoring strategies, and selection of intervention measures.

Acknowledgements

The authors would like to acknowledge the contributions of Mats Holmqvist (Invator AB), Sondre Nærland (Birdsview AS), Ørjan Nyberg (Aker Solutions), Megan O'Sadnick (SINTEF Narvik), and Magdalena Jadwiga Osmolska (Statens vegvesen) for their assistance during the laboratory testing, primarily related to data acquisition and measurements. Special thanks are also extended to Andrei Shpak and Frode Dalsaune (both from SINTEF Community) for their support in the fabrication and manufacturing of the mock-up specimens.

References

Belhadj, A., & Waldron, P. (1993). Investigation into cutting of bonded prestressing bars during demolition. *Roceedings of the Third International RILEM Symposium on Demolition and Reuse of Concrete and Masonry*, 295–306.

Bore, T., Taillade, F., Placko, D., & Himbert, M. (2010). CAPACITIVE PROBE FOR NON DESTRUCTIVE INSPECTION OF EXTERNAL POST-TENSIONED DUCTS: MODELLING BY DPSM TECHNIQUE. *AIP Conference Proceedings*, *1211*(1), 1983–1990. https://doi.org/10.1063/1.3362353

Buchner, S., & Lindsell, P. (2004). Controlled Demolition of Prestressed Concrete Structures. In *Demolition methods and practice* (p. 10). CRC Press.

Carsana, M., & and Bertolini, L. (2015). Corrosion failure of post-tensioning tendons in alkaline and chloride-free segregated grout: A case study. *Structure and Infrastructure Engineering*, *11*(3), 402–411. https://doi.org/10.1080/15732479.2014.887736

Cavell, D. G., & Waldron, P. (2001). A residual strength model for deteriorating post-tensioned concrete bridges. *Computers & Structures*, *79*(4), 361–373. https://doi.org/10.1016/S0045-7949(00)00150-4

Dai, L., Chen, Y., Wang, L., & Ma, Y. (2021). Secondary anchorage and residual prestressing force in locally corroded PT beams after strand fracture. *Construction and Building Materials*, *275*, 122137. https://doi.org/10.1016/j.conbuildmat.2020.122137

Dethof, F., & Keßler, S. (2024). Design of Concrete Mock-Ups with Complex Defect Scenarios Using Numerical Simulations. *Journal of Nondestructive Evaluation*, *43*(2), 59. https://doi.org/10.1007/s10921-024-01074-9

Felstead, A. E., & LINDSELL, P. (1981). Controlled demolition of a post-tensioned beam. *Transport Research Laboratory*, *15*(9), 20–23.

Giannini, E., R., Rivard, P., Kodjo, S. A., Wood, S. G., & Guimaraes, M. (2020). DEVELOPMENT AND TESTING OF NDE MOCKUP SPECIMENS WITH ASR. *ICAAR 2020 - 16th International Conference on Alkali Aggregate Reaction in Concrete*. ICAAR 2020 - 16th International Conference on Alkali Aggregate Reaction in Concrete, Lisboa, Portugal.

Hansen, B. (2007). Tendon Failure Raises Questions About Grout in Posttensioned Bridges. *MnDOT Post-Tensioned Bridge Preservation. Presentation, National Bridge Preservation Conference.*, *77*(11).

Holmqvist, M., Popescu, C., O'Sadnick, M., & Täljsten, B. (2024). *Special Inspection of PT – ducts on Gisund Bridge* (TEchnical Report 2024:01252; p. 47). Sintef Narvik AS.

Im, S. B., & Hurlebaus, S. (2012). Non-destructive testing methods to identify voids in external post-tensioned tendons. *KSCE Journal of Civil Engineering*, *16*(3), 388–397. https://doi.org/10.1007/s12205-012-1295-0

Kessler, S., & and Grosse, C. U. (2023). Hands-On Training of Non-destructive Testing Using a Mock-Up in the Curriculum of Civil Engineers. *Research in Nondestructive Evaluation*, *34*(5–6), 205–221. https://doi.org/10.1080/09349847.2023.2255538

Krause, M., Milmann, B., Mielentz, F., Streicher, D., Redmer, B., Mayer, K., Langenberg, K.-J., & Schickert, M. (2008). Ultrasonic Imaging Methods for Investigation of Post-tensioned Concrete Structures: A Study of Interfaces at Artificial Grouting Faults and Its Verification. *Journal of Nondestructive Evaluation*, *27*(1), 67–82. https://doi.org/10.1007/s10921-008-0033-5

Lau, K., Lasa, I., & Paredes, M. (2013). *Corrosion Failure of Post-Tensioned Tendons in Presence of Deficient Grout*. NACE-2013-2600.

Martin, J., Broughton, K. J., Giannopolous, A., Hardy, M. S. A., & Forde, M. C. (2001). Ultrasonic tomography of grouted duct post-tensioned reinforced concrete bridge beams. *NDT & E International*, *34*(2), 107–113. https://doi.org/10.1016/S0963-8695(00)00035-9

Menga, A., Kanstad, T., Cantero, D., Bathen, L., Hornbostel, K., & Klausen, A. (2023). Corrosion-induced damages and failures of posttensioned bridges: A literature review. *Structural Concrete*, *24*(1), 84–99. https://doi.org/10.1002/suco.202200297

Minh, H., Mutsuyoshi, H., & Niitani, K. (2007). Influence of grouting condition on crack and load-carrying capacity of post-tensioned concrete beam due to chloride-induced corrosion. *Construction and Building Materials*, *21*(7), 1568–1575. https://doi.org/10.1016/j.conbuildmat.2005.10.004

Nürnberger, U. (2002). Corrosion induced failure mechanisms of prestressing steel. *Materials and Corrosion*, *53*(8), 591–601. https://doi.org/10.1002/1521-4176(200208)53:8<591::AID-MACO591>3.0.CO;2-X

Oh, R.-O., Kim, H.-H., Choo, Y.-J., Park, S.-K., Rodrigazo, S. A., Yeon, J., & Park, C. G. (2024). Evaluation of Delaminations and Defects in Concrete Deck Using Non-Destructive Multi-Physical Scanning Technology. *Sustainability*, *16*(21). https://doi.org/10.3390/su16219225

Popescu, C., & Täljsten, B. (2020). *Design of mock-up specimne for void detection in tendon ducts*. Internal report (unpublished).

Popescu, C., Täljsten, B., Holmqvist, M., Langås, I., & Antonsen, R. (2024). *Condition survey of grouted tendons of a prestressed concrete girder bridge* (Technical Report 2024:01598; p. 37). Sintef Narvik AS.

Sharma, S., Osmolska, M. J., Hornbostel, K., Bathen, L., Novakova, I., & Geiker, M. (2024). Repair options for corrosion-damaged prestressed concrete bridges. *Nordic Concrete Research*, *70*(1), 99–123. https://doi.org/10.2478/ncr-2024-0004

Tinkey, Y., & Olson, L. D. (2007). Sensitivity Studies of Grout Defects in Posttensioned Bridge Ducts Using Impact Echo Scanning Method. *Transportation Research Record*, *2028*(1), 154–162. https://doi.org/10.3141/2028-17

Trejo, D., Been Im, S., Pillai, R. G., Hueste, M. B. D., Gardoni, P., Hurlebaus, S., & Gamble, M. (2009). *Effect of voids in grouted post-tensioned concrete bridge construction: Inspection and repair manual for external tendons in segmental, post-tensioned bridges* (Technical Report FHWA/TX-09/0-4588-2; p. 62). Texas Transportation Institute The Texas A&M University System College Station, Texas 77843-3135. http://tti.tamu.edu/documents/0-4588-2.pdf

Wang, L., Zhang, X., Zhang, J., Ma, Y., Xiang, Y., & Liu, Y. (2014). Effect of insufficient grouting and strand corrosion on flexural behavior of PC beams. *Construction and Building Materials*, *53*, 213–224. https://doi.org/10.1016/j.conbuildmat.2013.11.069

Wiggenhauser, H., Wöstmann, J., Schulze, S., Barry, K., Guimaraes, M., Scott, D., Lindberg, J., & LAreau, J., P. (2015). Non-destructive evaluation of steel-concrete mock-ups. *10th International Conference on NDE in Relation to Structural Integrity for Nuclear and Pressurized Components*, 969–975.

EXCON

https://www.sintef.no/prosjekter/2023/excon-gronn-forvaltning-av-konstruksjoner-for-infrastruktur/

Prosjektet er finansiert av Grønn Plattform ordningen som er et samarbeid mellom Forskningsrådet, Innovasjon Norge, Siva og Enova, og følgende deltagere: